University of Padua

Department of Information Engineering
Master's degree in Electronic Engineering

Effects of electric and thermal stress on polymeric solar cells based on P3HT:PCBM bulk heterojunction

Candidate:
Alessandro Maria Bazzega

Supervisor:
Andrea Cester
Co-Supervisor:
Nicola Wrachien

Academic year 2014/2015

Contents

Introduction

This thesis concentrates on the analysis of the effects of electric and thermal stresses on polymeric solar cells. The test samples are fabricated at the Danmarks Tekniske Universitet and based on a P3HT:PCBM blend as active layer.

In the first chapter are briefly reported the history and the current situation of the photovoltaics market, followed by a quick explanation of the working principles of generic inorganic solar cells. The next two chapters focus on organic electronics, first with a theoretical analysis of organic semiconductors that ranges from the chemical properties of the carbon atom to the conduction through organic semiconductors, and then with an overview of the structure and operation principles of organic solar cells.

In the second and last part of the thesis are the details of the actual work made on the cells. It starts with a complete characterization of the test samples that gives an idea on their performances, and continues with the electric and thermal stresses. Electric stresses include two different procedures. In the first one the stress voltage/current were increased over time, maintaining the duration of the stress steps constant. In the second one the stress voltage/current was kept the same and the stress steps were gradually increased. In thermal stresses two different temperatures were kept constant and the stress steps were progressively increased. The results are shown and a possible explanation to the behavior of the cells is suggested.

Chapter 1

Photovoltaics

1.1 History

The direct generation of electric power by light in a solid material is called *photovoltaic effect*, and it was discovered by William Grylls Adams and Richard Evens Day in the 1870s using selenium. The first silicon solar cell was developed in 1954 at Bell Laboratories. The project started in 1953, initially focusing on selenium, which was long known for showing photoelectric effect and had already been used to measure light intensity in photography. The electrical efficiency of the first selenium solar cell was just about 0.5%. The decision was made to deviate to silicon, and the next year a solar cell with efficiency of 5.6% was demonstrated. Over the following 20 years spacecraft and satellites power supplies became the main application of photovoltaics. Only in the early 1970s solar cells were reconsidered for terrestrial usage, as in those years the first commercial modules were released and large goverment-sponsored procurement plans began in the USA. In the next 10 years the new USA procurement plans together with the field testing of photovoltaics used mainly for remote-area telecommunications, led to a rapid improvement of the technology. A terrestrial solar cell industry was quickly established. Economies of scale and progress in technology reduced the price of solar cells dramatically.

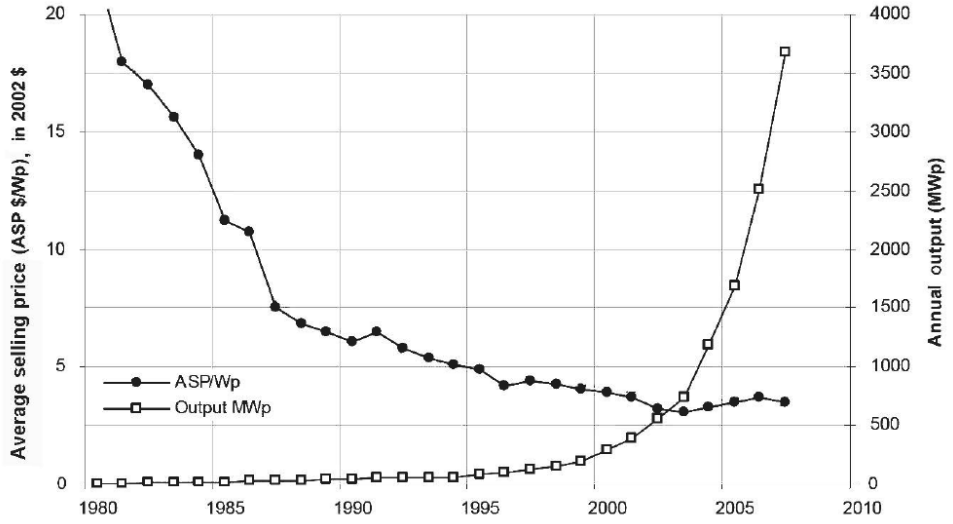

Figure 1.1: Average price per MW and output power over the years

1.2 Photovoltaics today

At the end of 2009, the world's cumulative installed PV capacity was more than 23 GW. One year later it was 40.3 GW and at the end of 2011 it was 70.5 GW. In 2012, the 100 GW mark was reached and by 2013, almost 138.9 GW of PV had been installed globally: an amount capable of producing at least 160 terawatt hours (TWh) of electricity every year. Europe remains the world's leading region in terms of cumulative installed

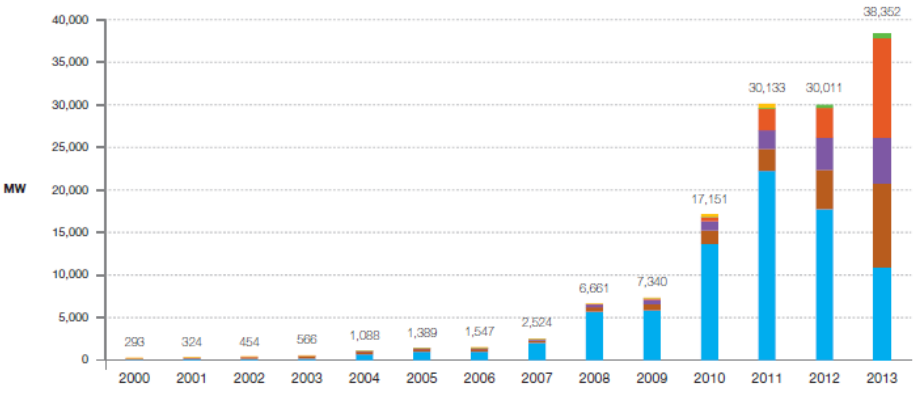

	2000	2001	2002	2003	2004	2005	2006	2007	2008	2009	2010	2011	2012	2013
RoW	88	56	80	77	29	10	105	42	76	80	284	508	n/a	n/a
MEA	n/a	n/a	n/a	n/a	1	0	0	1	1	22	55	125	365	383
China	19	5	19	10	10	8	10	20	40	160	500	2,500	3,500	11,800*
Americas	2	3	30	48	61	82	110	166	306	500	1,082	2,181	3,774	5,362
APAC	126	128	190	230	282	304	325	271	530	745	1,578	2,562	4,646	9,833
Europe	58	133	134	202	705	985	997	2,023	5,708	5,833	13,651	22,259	17,726	10,975
Total	**293**	**324**	**454**	**566**	**1,088**	**1,389**	**1,547**	**2,524**	**6,661**	**7,340**	**17,151**	**30,133**	**30,011**	**38,352**

RoW: Rest of the World. MEA: Middle East and Africa. APAC: Asia Pacific.
Methodology used for RoW data collection has changed in 2012.
**This number could be increased to 12,920 MW.*

Figure 1.2: New annual installation over the years

capacity, with 81.5 GW as of 2013. This represents about 59% of the world's cumulative PV capacity, down from 70% in 2012 and about 75% of the world's capacity in 2011. In fact in 2013 Asian countries took the lead and started to develop faster than traditional European markets. As a result, the cumulative installed capacity outside Europe almost doubled from 30 GW as of 2012 to close to 60 GW. China and Japan became the top PV markets in the world in 2013, and achieved the world's largest PV installation figure in one year with respectively 11.8 GW and 6.9 GW connected to the grid. After holding the world's top PV market position seven times in the last 14 years, Germany was only fourth in 2013 with 3.3 GW, and yet still by far the largest European market. The UK was the second European market with 1.5 GW. Italy, which was the second European market in 2012, installed more than 1.4 GW in 2013, down from 3.6 GW the year before and 9.3 GW in 2011.

Europe's strong PV market development until 2012 was the result of a few countries taking the lead year after year, with German policymakers showing a constant commitment to supporting the development of PV. Spain and the Czech Republic demonstrated that overheated market development can produce a boom in one year and a bust in the next, as a result of pressure from conventional energy producers and policymakers concerned about the rapid growth of the market. The instability of markets in Europe leads to the important conclusion that, with the exception of a comparably soft landing of

the market in Germany, no country that experienced a serious PV boom once has so far succeeded in restoring market confidence. On the contrary, policymakers seem to have ensured that in these countries PV would not be allowed to reach the same market levels reached previously. This was the case in Spain, Czech Republic, Slovakia, Bulgaria, and most probably in Belgium and Italy. Overall, the future of the European market is uncertain for the coming years. The drastic decrease of some programmes will push some markets down in 2014, with a limited number of emerging markets in Europe that could offset any major decline. Given these new conditions, the short-term prospects for the European markets are stable in the best case, and could even decline. In the Low Scenario, without support from policymakers for PV, the transition to a cost-competitive PV market driven less by financial support schemes could be difficult over the five years to come, with a rather low market in Europe (around 6-8 GW). In the High Scenario, the market could stabilise in 2014 and grow again from 2015 onward, driven by the approaching competitiveness of PV and emerging markets in Europe.

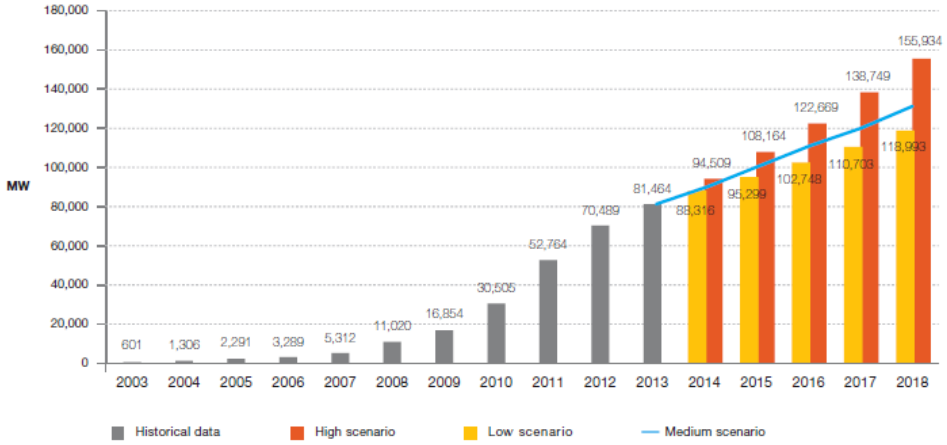

Figure 1.3: Forecast of future scenarios for the European market until 2018

1.3 Solar cells

1.3.1 Solar spectrum

The solar radiation reaches the outside of earth's atmosphere with a power density of $1353W/m^2$. The vast majority of the solar spectrum ranges from a wavelength of 150nm to 4000nm, as shown in 1.4. The solar radiation is partially absorbed during its passage through the atmosphere, and about 25% of it is just reflected toward the space. Absorption is caused by gases and dust, which heat up and emit infrared in all directions, and of course it increases with le length of the path through the atmosphere and therefore with the mass of air through which the radiation passes. For a thickness l_0 of the atmosphere, the path length of the radiation which comes from the sun with an angle α relative to the earth's surface is given by

$$l = \frac{l_0}{sen(\alpha)}$$

The ratio l/l_0 is called *air-mass coefficient* (AM), and it characterizes the solar spectrum resulting that pass through an air thickness of length l. Outside the atmosphere AM = 0 (usually referred as AM0), and at earth's surface - with incidence of 90 degrees - AM = 1 (AM1). The standard used in lab test for measuring the solar cells efficiency is an halfway AM1.5, which corresponds to an angle of 42 degrees. The total intensity of the solar radiation that reaches the earth's surface with a cloudless sky (given that the spectral distribution is modified from the absorption) is about $1000W/m^2$, or $100mW/cm^2$, which is the unit of measure for the solar radiation, the *Sun*. The solar spectrum narrows, as the wavelength range vary between 200nm and 2500nm, and it is distribute as 45.6% infrared, 48% visible and 6.4% ultraviolet.

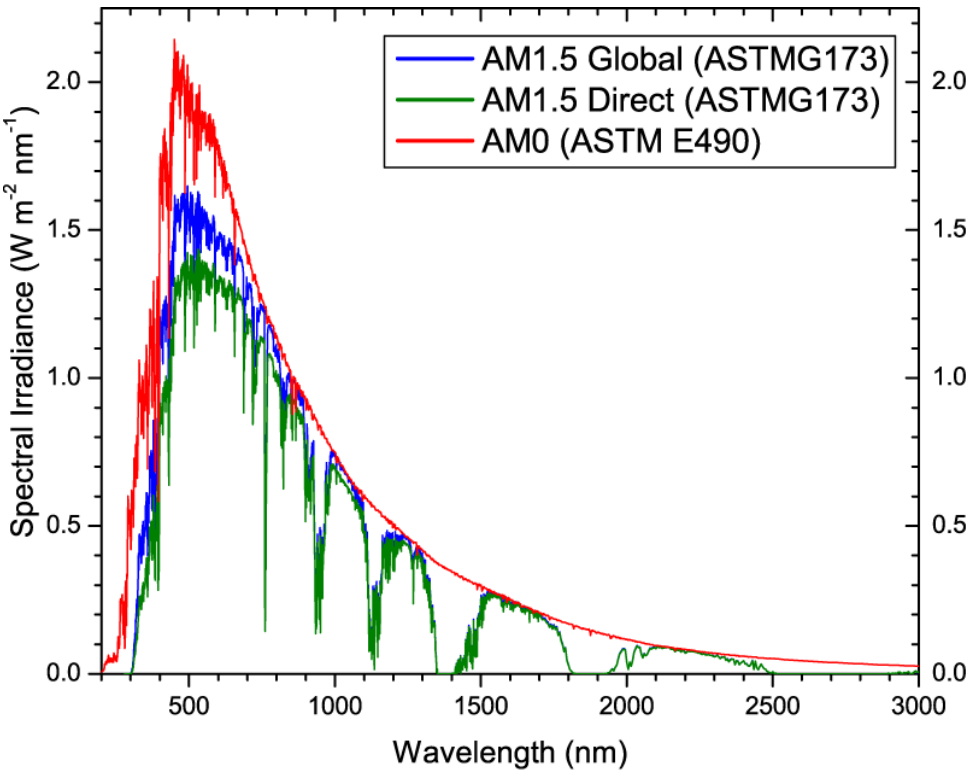

Figure 1.4: Solar spectrum AM0 and AM1.5: The AM1.5 Global spectrum is designed for flat plate modules and has an integrated power of 100 mW/cm2 (1Sun). The AM1.5 Direct spectrum is defined for solar concentrator work. It includes the the direct beam from the sun plus the circumsolar component in a disk 2.5 degrees around the sun.

1.3.2 pn-junctions

The first 1954 solar cell was made from a single crystal of silicon, accurately doped to form a p–n junction.

Even today most solar cells are made of semiconductors, that is a material in which the energy gap between the top of the valence band[1], completely filled with electrons, and the bottom of the conduction band[2], empty, is narrow (tipically a fraction of an

[1]the highest energy band in which electron are present at 0°K
[2]the lowest empty energy band at 0°K

electron volt to a few electron volts). The propriety that made semiconductors essentials in today's technology is the fact that their conductivity critically depends on the type and concentration of impurities. An *n-type* semiconductor is made by adding *donor* impurities, which add energy levels just below the bottom of the conduction band and move the fermi level upward. Electrons in those leves can easily be stimulated to go up to the conduction band. Adding *acceptor* impurities, on the other hand, leads to the creation of a *p-type* semiconductor, in which the levels added are just above the valence band, in which the holes of the acceptor levels can easily descend.

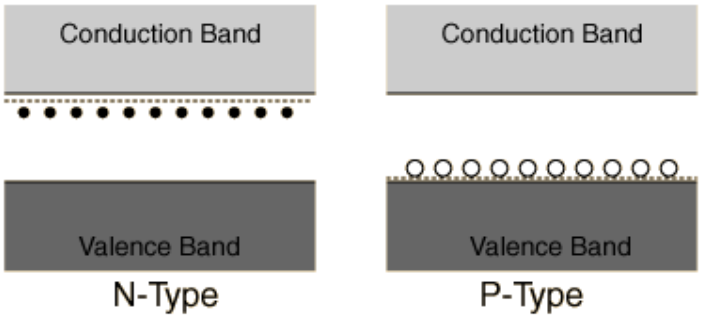

Figure 1.5: Doped semiconductors

When a p-type and a n-type semiconductor are brought together to form a single system, the difference in electron concentrations causes electrons to flow from the n-type semiconductor to the p-type and holes to flow from the p-type semiconductor to the n-type (*diffusion*). As a result, the uncompensated dopant atoms cause an electric field which creates a potential barrier qV_{bi} between the two materials, equal to the difference between the fermi levels of the separate semiconductors. At equilibrium the flow of electron from diffusion and the flow of electrons due to the electric field (*drift*) are balanced, so the net current is zero.

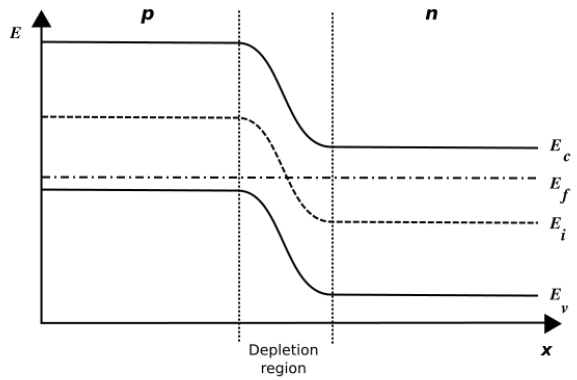

Figure 1.6: pn-junction band diagram

1.3.3 Solar cells

The structure of a generic solar cell, as stated before, it the one of a pn-junction. In the first 1954 cell the n-side of the junction was very thin and highly doped to allow light to

come to the p–n junction with very little attenuation, and the lateral electric conduction is high enough to collect the current to the front contact through an array of silver fingers.

According to the theory of quantum transitions an incident photon with energy greater than the gap energy of the semiconductor material can be absorbed and create an electron–hole pair. Because of the built-in electric field, which points towards the p–type region, the electrons drift into the n–type region, whereas the holes stay in the p–type region. The current generated by the sunlight that flows when the two terminals are connected together is called *short circuit current* (Isc), and it is the maximum current that the cell can supply. On the contrary, if the two regions are not connected externally, the charges accumulated in the two regions generate a potential across the junction capacitance. The potential becomes a forward voltage, and when an equilibrium is established between the flow of electrons this voltage is the *open-circuit voltage* of the solar cell under illumination (Voc). The basic model of a solar cell is a (light controlled) current generator in parallel with a diode:

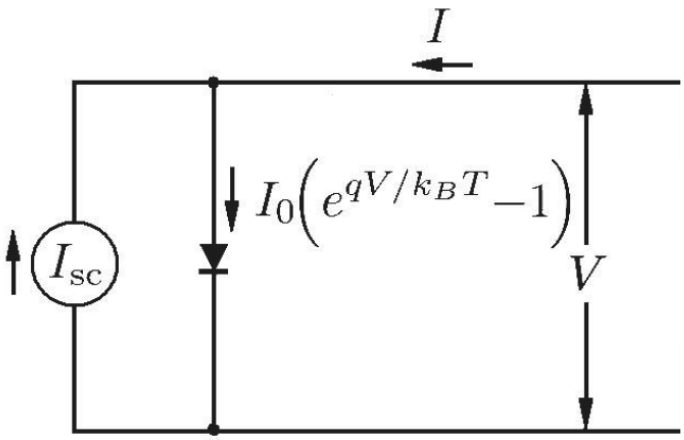

Figure 1.7: Electric model of a solar cell.

The solar cell equation is therefore:

$$I = I_{sc} - I_0\left(e^{\frac{qV}{k_BT}} - 1\right)$$

from which, imposing a null current, the relation between Isc and Voc is found:

$$V_{oc} = \frac{k_BT}{q}\ln\left(\frac{I_{sc}}{I_0}\right)$$

The figures of merit that characterize the performance of the solar cells are usually Isc, Voc and a few others. In particular:

- **Fill factor**
- **Efficiency**

The Fill Factor is the ratio between the maximum output power of the cell, defined as the power supplied when $V = V_M$ such that $\frac{dP_{out}}{dV_{out}}(V_M) = 0$, and the product of Voc and Isc.

$$FF = \frac{P_{max}}{V_{oc}I_{sc}}$$

It is an *ideality index* that gives information on how far the cell is from ideality. A cell with FF = 1 is an ideal cell, and its I_{out} remains equal to Isc until $V_{out} < V_{oc}$. When $V_{out} = V_{oc}$ the current drops to zero.

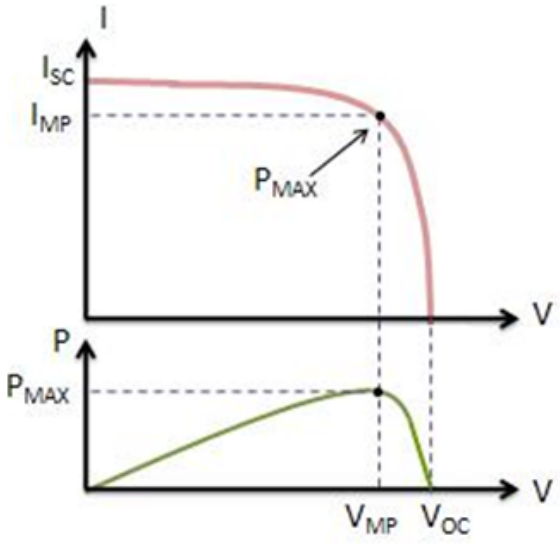

Figure 1.8: IV Curve and the corresponding P-V curve.

The efficiency can be intended as *quantum efficiency* (external or internal) or as *electric efficiency*. The External quantum efficiency is the ratio between the number of electron-hole pairs that are extracted and the number of incident photons, while the internal is the ration between the number of electron-hole pairs that are extracted and the number of *absorbed* photons. They both depends on the probability of the recombination of the electron-hole pairs.

The electric efficiency quantifies the ability of the cell of convert optical power into electric power, and it is thus defined as

$$\eta = \frac{P_{max}}{P_i} = \frac{V_{oc} I_{sc} FF}{P_i}$$

with P_i the incident optical power. The efficiencies of an ideal solar cell are equal to 1.

Chapter 2

Organic Electronic

While polymers have been known and utilized for many decades, polymers with the intrinsic properties of semiconductors and metals are a relatively recent phenomenon. Early studies recognized that a key feature of organic materials was a backbone consisting of alternating single and double bonds resulting in a $\pi - coniugatednetwork$ which led to a relatively small energy gap. Initially these polymers were unstable in air and not readily processed, but over the past decades major advances have occurred in the synthesis of new forms that enable processing under a broad range of conditions. Research in organic electronics has witnessed similar explosive growth. The notion of creating electronic circuits and devices on plastic platforms, as apposed to a silicon foundation, provides researchers the possibility of circumventing issues such as cost, weight, widespread adoption and fragility. Global development of small molecules and polymers that are used throughout the field has accelerated, primarily in response to these advantages. The materials function as semiconductors, conductors and light emitters finding use in a myriad of applications such as smart windows, electronic paper, printed electronics inks, low-cost flexible photovoltaic devices and lasers.

2.1 Organic semiconductors

The term "organic" refers to carbon-based molecules, which usually also contain hydrogen, oxygen, nitrogen and various other elements. Organic compounds are divided in:

- molecules, in which the structure and the molecular mass are well known
- monomers, composed by atoms arranged in such a way that it is easy for them to combine recursively
- oligomers, sequences of monomers with a defined length
- polymers, which are sequences of monomers (virtually infinite) whose length and molecular mass are not defined.

2.1.1 Carbon orbitals

In carbon, four electrons occupy the valence orbitals *2s* and *2p*, which can contain a maximum of 8 electrons. Following Pauli exclusion principle, valence electrons should fill

the 2s orbital and half-fill the $2p_x$ and $2p_y$ orbitals ($2s^2 2p^2$), so carbon should only be able to form two bonds (2.1).

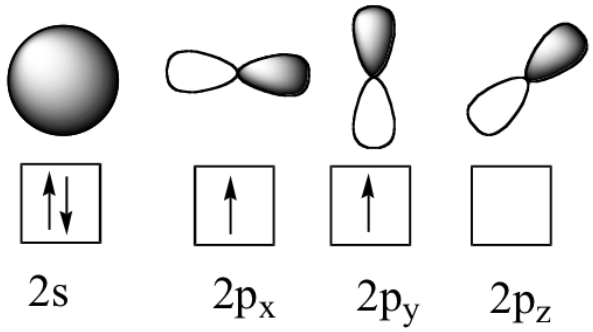

Figure 2.1: Electrons disposition folloqing Pauli's principle

Actually, though, in the majority of carbon-based compounds it forms four bonds: this is due to the fact that the energy levels of the 2s and 2p orbitals are sufficiently near to allow electrons from the 2s to easily climb into the 2p orbitals, since the spent energy is compensated by the energy released by the two new bonds. This mechanism is called *hybridization*. The total energy of an hybridized system is lower than the energy of the original one since the orbitals adjust themselves in a more stable configuration, where they are isoenergetic. The new orientation of each orbital is the one that maximizes the inter-nuclear distances and minimizes repulsion and the system energy. In the carbon atom there are three possible ways for orbital to hybridize, that differ for the number of p-orbital involved. They are

- sp^3 hybridization
- sp^2 hybridization
- sp hybridization

In sp^3 hybridization the $2s$, $2p_x$,$2p_y$ and $2p_z$ orbitals concur in the formation of four new tetrahedral orbitals, each one showing two asymmetric lobes, fixed at an angle of 109° between each other. Electrons are arranged as one in each sp^3 orbital, therefore carbon can form four bonds with just as many atoms.

In sp^2 hybridization three new orbitals replace the $2s$, $2p_x$ and $2p_y$ orbitals and dispose with a 120° angle on a plane orthogonal to the $2p_z$. This is a configuration that often occurs when a double bonding between two atoms is present. In such case the sp^2 orbitals form a σ-bond, while the $2p_z$ contribute in the creation of a π-bond, weaker than the former.

The last is the sp hybridization, in which only the $2s$ and the $2p_x$ transform into hybridized orbitals. They dispose symmetrically in opposite directions on a straight line orthogonal to the plane defined by the remaining 2p orbitals. This configuration can lead to a triple bond, where the σ-bond is made by the sp orbital, while the two 2p orbitals concur in the π-bonds.

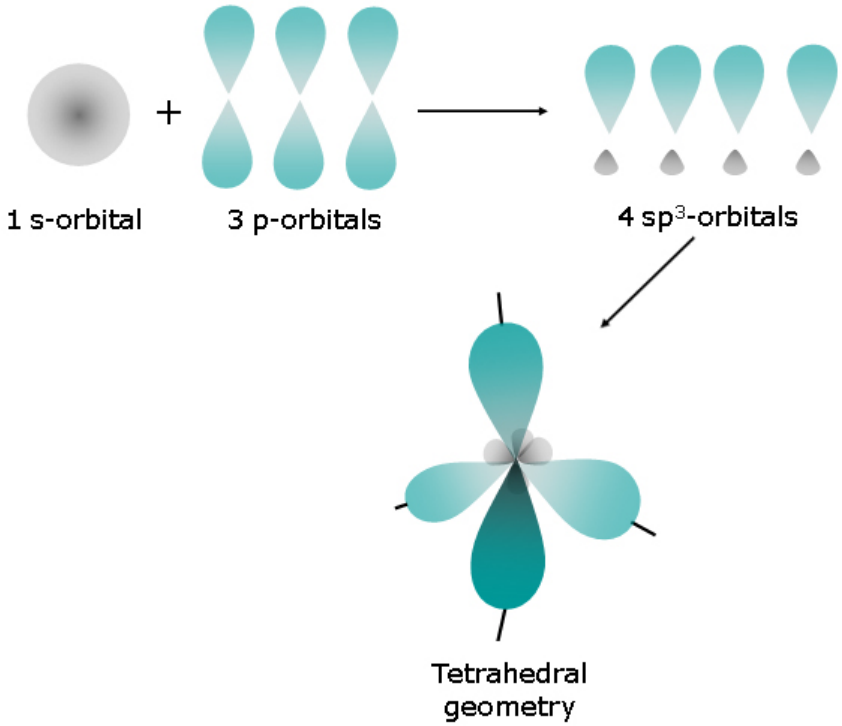

Figure 2.2: sp^3 hybridization

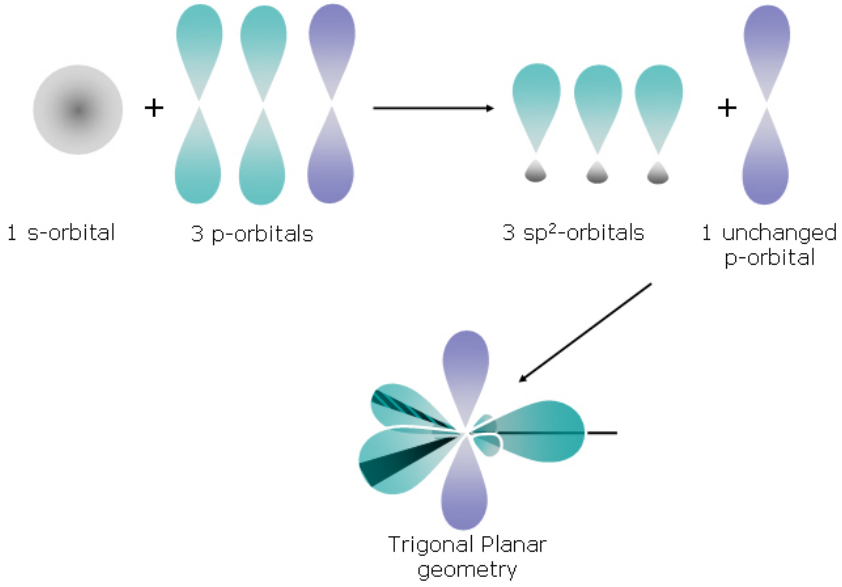

Figure 2.3: sp^2 hybridization

2.1.2 Molecular and Inter-molecular orbitals

A conjugated system is a structure of atoms alternating single and multiple bonds in which the non-hybridized p-orbitals - and their electrons - are delocalized over the entire system, due to the overlapping of the p-orbitals that creates a bridge between adiacent bonds.

If we consider a conjugated system with 2N carbon atoms with a cyclic or chain structure, they form N double bonds alternated to N single bonds. Each single bond is

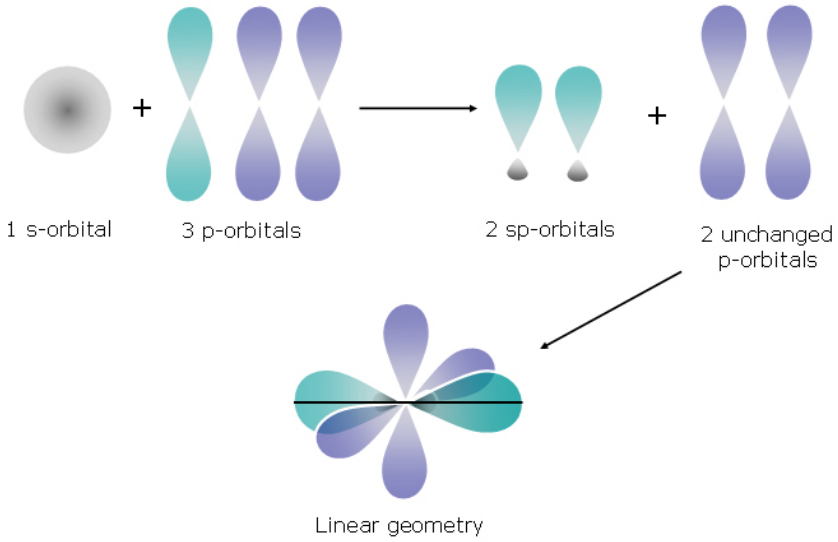

Figure 2.4: *sp* hybridization

associated with two localized molecular orbitals, σ and σ^*, and both the electrons occupy the lowest σ level with opposite spin. The remaining 2N atomic p-orbitals become N π-orbital and N π^*-orbitals[1]. Two of these orbitals are very significant:

- the *Highest Occupied Molecular Orbital* (HOMO) is the highest orbital that contains at least one electron at 0 K
- the *Lowest Unoccupied Molecular Orbital* (LUMO) is the lowest empty orbital at 0 K

These two energy levels are the organic equivalent to the conduction and valence band. The gap between HOMO AND LUMO corresponds to the energy gap of inorganic semiconductors.

When two molecular orbitals are put together they combine into a more complex structure, the Inter-molecular orbital. In a lattice made by organic conjugated molecules, each π and π^* orbital splits in a dense stack of levels, whose number increase with the number of molecules involved. HOMO and LUMO undergo the same process, and they become respectively the *Holes Transport Band* and the *Electrons Transport Band*

The main difference between organic and inorganic energy bands is that electron delocalization in organics semiconductors does not extend to the entire lattice volume, but it is mostly limited to the single molecules: an electron is more likely to be bound to its original molecule than to the near ones. This weak delocalization leads to a lesser separation between molecular orbitals, thus unlike the conduction and valence bands, whose width can be about 20eV, the HOMO and LUMO widths are usually less than 1eV.

Another important difference is that the energy of the inter-molecular bonds, in organic semiconductors, depends on the mutual orientation of the molecules. A wider orbitals overlapping leads to stronger bonds, since it means a greater delocalization.

[1]All π-orbitals have comparable energies, lower than the one of the p-orbital but higher than the σ level. The energies π^*-orbitals are bewteen the p-orbital and the σ^* level

2.2 Charge transport

Considering an organic lattice at equilibrium, electrons occupy the lowest energy bands following Pauli's principle. When photons or phonons interact with the lattice they can be absorbed by a molecule, gaining enough energy for a transition to an excited state. The energy levels of a molecule depend on a combination of the molecular orbital energy and the vibrational state energy.

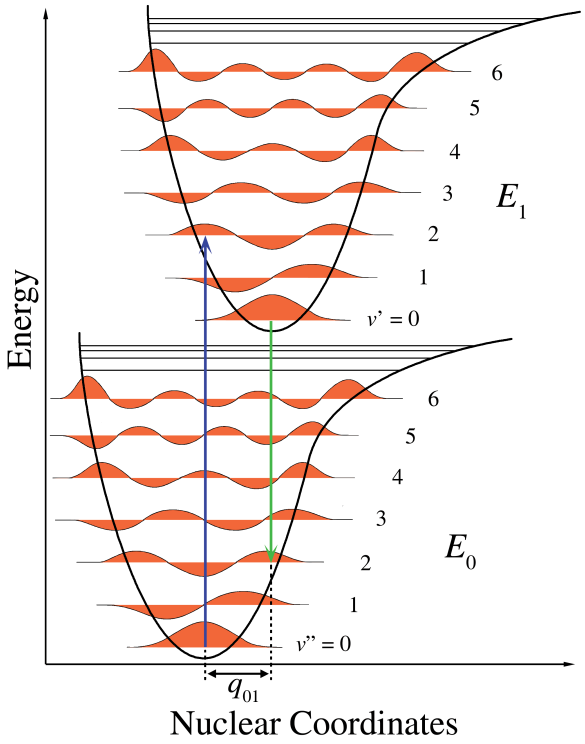

Figure 2.5: Electronic and vibrational states of a molecule. Not all vibrational transitions between different orbitals have the same probability.

Franck-Condon's Principle says that during electronic transitions[2] the inter-nuclear distance of the molecule is kept unchanged. This is due to the fact that electronic transitions are way faster than the molecular vibration, so the nuclei can be assumed as stationary. This principle implies that not all vibrational transitions[3] between different orbitals have the same probability. A transition is likely to happen only if the wave functions of the two states overlap considerably, as shown in fig. 2.5.

2.2.1 Excitons

The electrons of a molecule in ground state occupy the levels of the HOMO band, while the LUMO band is empty. If the molecule is given enough energy (i.e. by the absorption of a photon) it can rise into an excited state, which means that an electron from the HOMO band moves to the LUMO band. That same electron can now easily pass from its π^*-orbital into the π^*-orbital of a near atom, leaving a hole behind that charges the

[2]Transition between orbitals
[3]Transition between vibrational states

atom positively. The molecule is still neutral, but it now contains two electrically charged regions that induce an alteration of its structure. The bound state of the electron and the hole, attracted to each other by the Coulomb force, is called *exciton*. It is a quasiparticle that exists in insulators, semiconductors and in some liquids: even if electrons in inorganic semiconductors seem to become "free" as soon as they move into the conduction band, actually the creation of an electron-hole pair leads to the creation of a very weak exciton.

Excitons are categorized according to their energy:

- **Wannier-Mott excitons** distinguish for their very low energy. They are usually found into inorganic semiconductors, since their high dielectric constant and carrier concentration reduces the coulomb attraction between electrons and holes. Thermal energy can easily break this weak bond, separating the pair permanently.

- **Frenkel excitons** are high-energy excitons typical of materials with low dielectric constant and carrier concentration, such as organic semiconductors. The bond between electron and hole is strong, and since thermal energy can't break it they tend to recombine.

An exciton can move into other molecules, but since it is a neutral quasiparticle this process doesn't imply a charge transfer. The molecule can relax to the ground state giving its energy to the nearest one, where a new exciton is created. This *energy transfer* can happen in two ways:

- Forster Resonance Energy Transfer (FRET): FRET can only happen if the emission spectrum of the excited molecule partially overlaps the absorption spectrum of the relaxed one, so that the released energy can excite it. The two molecules can be seen as oscillating dipoles: if their resonance frequencies are close enough the excited one can give up its energy to stimulate the other. The efficiency of the Forster transfer follows a $distance^{-}6$ law, which make it appreciable for inter-molecular distances below 10nm.

- Dexter Energy Transfer: If the molecular orbitals overlap and the inter-molecular distance is small enough, the excited electron can pass into the other orbital, while an electron from the ground state of the acceptor molecule is transferred to the donor. The efficiency of the Dexter transfer decays exponentially and dominates over FRET only for distances of a few nm

2.2.2 Polarons

The electron and the hole of an exciton are delocalized over the molecule, so they can move freely inside of it. It could happen that the electron (or the hole) moves to a nearby molecule thanks to the orbital overlapping, and go far enough for the thermal energy to break the bonds of the electron-hole pair and leaving two *charged excitons*. Their charge induce a deformation of the structure of their molecule, which relax to minimize the system energy. The combination of the electric charge and the induce structural deformation is called *polaron*. The formation of a polaron is not an instantaneous process: the charged exciton has to stay inthe molecules for at leas 100fs for a complete polaron to

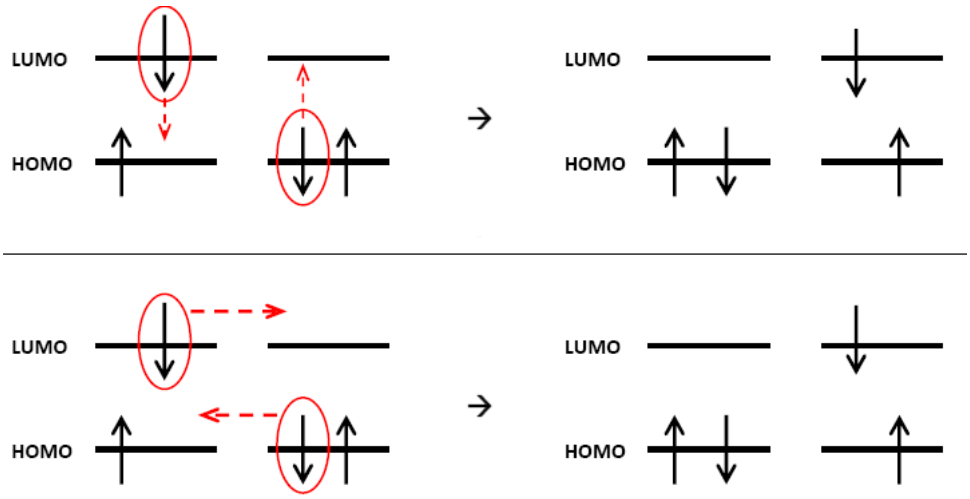

Figure 2.6: Forster energy transfer (top) and Dexter energy transfer (bottom)

establish. In the first fs the electrons clouds polarize (electron polaron) and redistribute. Lengths and angles of the molecular bonds are stabilized after 10fs (molecular polaron), and after 100fs the lattice deformation is complete (lattice polaron). The overall energy decrease amount to more than 1eV.

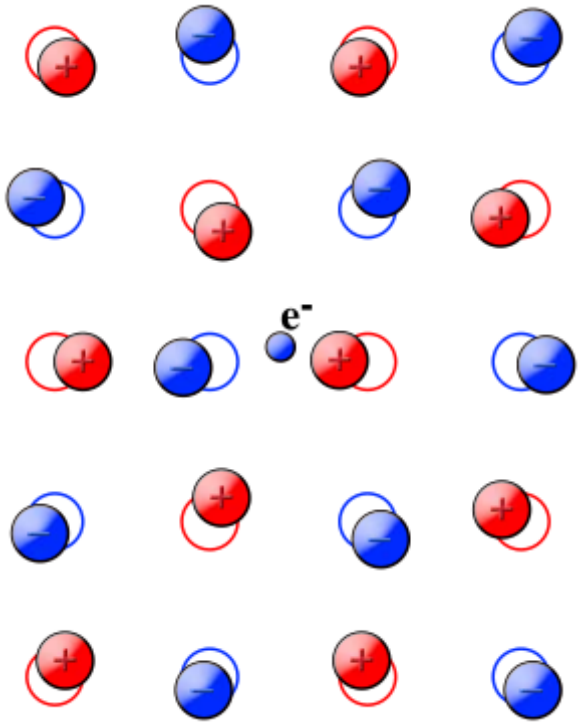

Figure 2.7: Deformation induced by a polaron

A polaron can move between molecules like an electron, thanks to the orbitals overlap. Its deformation move alongside, since it is part of it, and the molecules return to their previous structure after the polaron is gone.

2.2.3 Transport

Since electrons are delocalized over the entire molecule, the *intra-molecular transport* is theoretically very efficient. The molecule can be seen as a one-dimensional quantum well, where the state of the electron is fully described by a wave function. As long as the electron remains inside the molecule, its energy and momentum are kept unchanged, so it avoids collisions while moving. Landauer's model can be used to describe conduction inside an organic molecule, and the resulting conductance, the *quantic conductance*, turns out to be constant and independent of the length of the molecule. Although intra-molecular conduction could apparently result quite efficient providing long enough polymers, actually a single impurity would break the periodicity of the molecule, and its resistance would become the series of two quantum resistance. Since impurities are very common in organic semiconductors, the actual resistance of a molecule is much greater.

Inter-molecular transport happens when orbitals from different molecules overlap, and it is mainly due to an electric field. This transport is conditioned by the properties of the organic materials: the low mobility causes electrons to move at a limited speed, thus giving enough time to establish a molecular (or even lattice) polaron. Charge transport in organic semiconductors is then governed by polarons instead of electrons, and while it is still based on drift and diffusion as in inorganic semiconductors, the physical process behind them is not totally understood. The *variable-range hopping model* can be used to explain the conduction: molecules are approximated as trap states in which the polaron is weakly restricted, and it can jump from a trap to another with comparable energy only by overcoming the potential barrier between them. The wall can be surpassed by tunnel effect or, if the temperature is high, by the contribution of the thermal energy alone. In either way, applying an electric field lower the potential wall and ease the conduction.

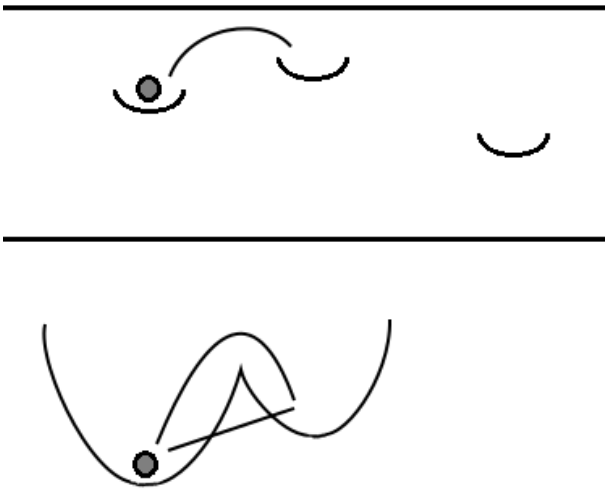

Figure 2.8: Carrier transfer following hopping model.

2.3 Mobility

The concept of mobility can be extended to organic semiconductors, since the relation between speed and electric field still stands. Unlike inorganic semiconductors, mobility is anisotropic in organic semiconductors, meaning that it depends on the orientation and the morphology of the molecules. Since inter-molecular transport relies on the orbital overlapping, a crystal structure in which molecules are close together and the empty space is kept to a minimum leads to a higher value of mobility. Amorphous structures, on the other hand, can reduce the overlapping to the point where the material is considered an insulator. In fact most semiconductors show a polycrystalline structure, composed of many crystallites (grains) of varying size and orientation, and the mobility is lower than in crystal structures but higher than in amorphous ones[4].

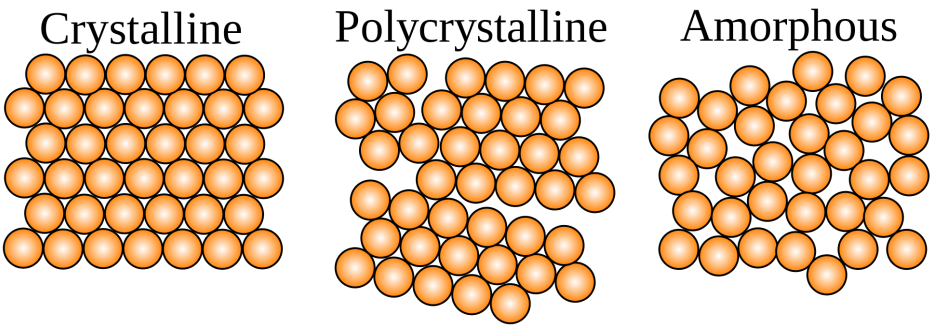

Figure 2.9: Possible lattice structures of a semiconductor.

The orientation also strongly contributes to the mobility: this is due to the fact that in organic molecules and polymers one side is usually greatly longer than the other, so depending on their disposition and orbital overlapping, the conductivity over each direction remarkably changes. Considering fig. 2.10, where it's shown a pentacene molecule, the maximum in orbital overlapping and thus in mobility is found when molecules are filed along the $\pi - \pi$ axis. Contrarily, conductivity between molecules aligned along the primary axis is poor and along the secondary axes the results depend on the presence of substituents which could increase the distance between orbitals.

Polymers can be influenced by the orientation more than morphology. An amorphous polymer can show an higher mobility than a crystal one, if the orientation of the former maximize conduction.

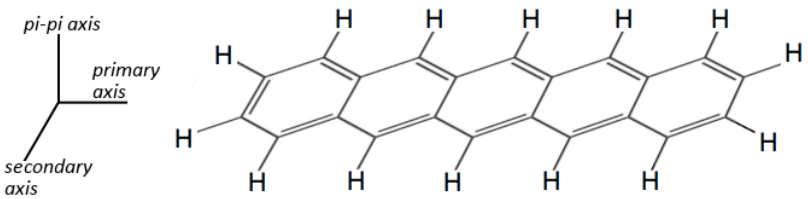

Figure 2.10: Pentacene molecule.

[4]Usually below $1cm^2/Vs$

2.3.1 Band diagram

The bands of organic semiconductors are not clearly separated. The band gap contains several permitted states, and the difference between the trap states and the permitted levels of the conduction and valence bands is their mobility. Energy levels of the permitted bands are delocalized over the molecule, so the charge carrier is almost free when inside them and has high mobility. Trap states, on the other hand, are strongly localized over the defect from which they are born, so the trapped charge carrier is bound to it. This means that trap states have basically null mobility.

Since the bands are not easily discerned from the energy of the states, in organic semiconductors they are usually defined by their mobility. The conduction and valence band borders are therefore the levels that separate the high-mobility states from the low mobility states of the band gap, and they are not necessarily the same as the HOMO and LUMO. The band gap itself can therefore be defined in function of energy or mobility:

- Optical Band Gap: the minimum energy required to ionize an electron an take it to the next free energy level, which could not be part of the transport band.
- Mobility Gap: the difference between the energy levels corresponding on the mobility threshold that separates high-mobility states from low-mobility ones.

2.4 Doping

The number of impurities in organic semiconductors is high enough that the intrinsic doping can reach concentrations up to $10^17 impurities/cm^3$, thus any further addition would make the material a conductor. In organic materials a *doping* process aims at the oxidation or the reduction of a molecule, which leads respectively to a p and a n semiconductor. Differently from the inorganic context, though, "n" and "p" assume a different meaning:

- **n-type** refers to a material in which is possible to inject, transport and collect electrons
- **p-type** refers to a material in which is possible to inject, transport and collect holes

A material in which both electrons and holes can be injected, transported and collected is called *ambipolar*.

2.5 Current in organic semiconductors

Applying a voltage to a semiconductor film between two metallic electrodes causes a current to flow. The charge transport mechanism consist of two phases:

- the carriers injection from the electrode to the film
- the charge transport through the semiconductor

The sum of the time needed by each phase defines the necessary time to move a charge carrier from one electrode to the other. The transport mechanism is limited by whichever phase takes the longer time.

Injection limited conduction

If the injection time is much greater than the transport time it means that the work function of the metal is not aligned with either the HOMO or the LUMO band of the semiconductor. The semiconductor can be seen as free of charges, since they cross through it in a negligible time.

For a carrier to overtake the potential barrier there are two ways, similar to those of the hopping model:

- **Fowler-Nordheim Injection**: if the barrier is high electrons must pass through it by means of *tunnel effect*. The Fowler-Nordheim current (or tunnel current) is given by

$$J_{FN} = A\varepsilon^2 e^{-\frac{B}{\varepsilon}} = \frac{A}{L^2} V^2 e^{-\frac{BL}{V}}$$

  where A and B are constant defined by the barrier properties and other physical constants.

- **Richardson-Schottky injection**: electrons can climb over a low enough barrier just thanks to their thermal energy. This current is strongly dependent on the height of the barrier, and it is defined as:

$$J_{RS} = J_0 e^{\alpha\sqrt{E}}$$

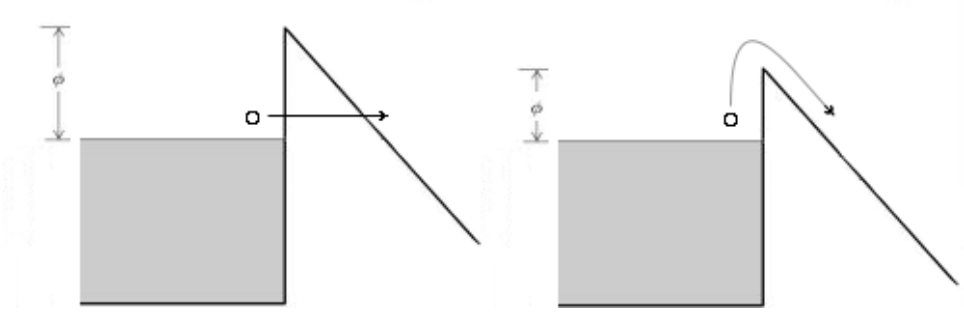

Figure 2.11: Fowler-Nordheim Injection (left) and Richardson-Schottky Injection (right)

Semiconductor limited conduction

If the transport time is much greater than the injection time, conduction only depends on the properties of the semiconductor film. Depending on the ratio between injected and intrinsic free charge carriers, two different models can be used to describe the conduction:

- **Ohmic model**: this is mostly the case of inorganic semiconductors, in this model the injected carriers are negligible compared to the intrinsic free carriers. The electric field is a constant since the total charge is almost null, and the relation between current and voltage is simply

$$J = qN_D\mu\frac{V}{L}$$

  As soon as the injected charge becomes significant this model loses its accuracy.

- **Space charge limited model**: this model is the more suitable for organic semiconductors, since it assumes that the intrinsic free charge in the film is almost null compared to the injected one. With a few simplification hypothesis[5] the relation between current and voltage can be extrapolated:

$$J = \frac{9}{8}\mu\varepsilon\frac{V_D^2}{L^3}$$

It can be seen that the relation is not linear, but rather parabolic. This is because the electric field now depends on the position, since the absence of intrinsic free charge.

From the previous relation can be determined the semiconductor resistance, and a capacitance can be associated to the total charge stored inside the film. These two elements compose a basic model of the impedance of an organic semiconductor:

$$R_D = \frac{V}{J} = \frac{8L^3}{9\mu\varepsilon V} \qquad r_D = \frac{dV}{dJ} = \frac{4L^3}{9\mu\varepsilon V}$$

$$C_D = \frac{dQ}{dV} = \frac{3}{2}\frac{\varepsilon}{L}$$

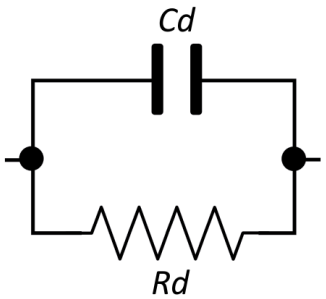

Figure 2.12: Impedance model of an organic semiconductor

Considering the effects of the surface and deep defects the previous equation are still correct, but the mobility is now a defect-dependent *effective mobility* given by

$$\mu_{eff} = \frac{\mu n_C}{n_C + n_D + n_T}$$

for each carrier type, where

[5]
- Absence of barriers at the interfaces between electrodes and film
- Negligible intrinsic free carriers
- Absence of doping
- Absence of defects
- Carriers mobility constant through the film
- Only one type of carriers exist in the film

– n_C is the number of electrons in the transport band

– n_D is the number of occupied surface defects

– n_T is the number of occupied deep defects

2.6 Organic Diode

An organic diode is a system composed by an organic semiconductor put between two ohmic metal electrodes, one with a work function similar to the one of the conduction band (cathode), and the other with work function similar to the valence band (anode).

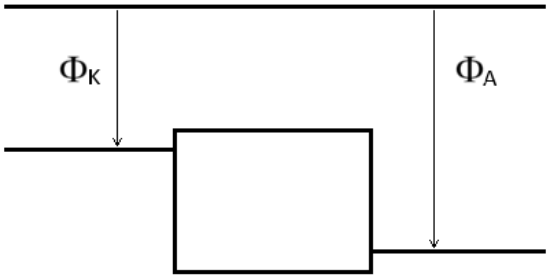

Figure 2.13: Organic diode band diagram.

In short circuit conditions, in the organic film there is a voltage drop equals to the difference of the two work functions, and the bands bend so cathode and anode reach are aligned. When an negative voltage is applied the bands bend, but the barrier at the interfaces are almost high as the band gap and thus they prevents a good carrier injection. In these conditions the diode can be viewed as an insulant.

When applying a positive voltage less than the difference between the work functions the magnitude of the bending decrease, and becomes null when $V = \phi_A - \phi_K$. Increasing further the voltage cause the bending to invert, and the carriers can be injected in the semiconductor. The voltage drop across the semiconductor is given by $V = V_{applied} - \phi_{AK} = V_{applied} - V_{ON}$, and the current is

$$J = J_0 \left(\frac{V_{applied} - V_{ON}}{V_0} \right)^{\nu}$$

Chapter 3

Organic Photovoltaics

The interest in the field of organic solar cells grew considerably in the last decades, mainly because of the recognition that organic semiconductors could possibly offer a low cost approach to flexible large area solar cells. Their potentialities were enough for research to overcome the initial obstacles of OPV, such as poor chemical stability and a very low efficiency. However, a better understanding of the nature of OPV and the advancement of manufacture techniques led in recent years to a great improvement in reliability and performances which is still ongoing.

The simpler structure for a solar cell is a thin organic film enclosed between a transparent anode (usually ITO) and a cathode with a low work function. When in equilibrium conditions, the difference between the work functions produces an electric field directed from the cathode to the anode.

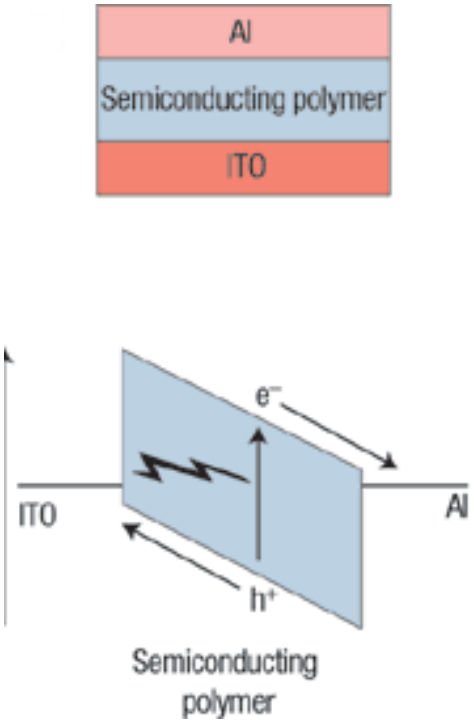

Figure 3.1: Single layer organic solar cell.

A photon absorbed by the cell induce the generation of an exciton which then, if

the electric field is strong enough, is separated into two opposite polarons that flow to the respective contacts: the hole to the anode and the electron to the cathode. The electric current that a photovoltaic solar cell delivers corresponds to the number of charge carriers that are effectively collected at the electrodes, that is the product of the number of photons that reach the cells multiplied for the efficiency of absorption, separation and transport (to the electrodes):

$$\eta = \eta_{abs}\eta_{sep}\eta_{out}$$

The minimum energy necessary for a photon to be absorbed corresponds to the difference between the LUMO and HOMO levels. The electron-hole pair is still bound into an exciton thanks to the Coulomb attraction, and the energy of this bond is usually 0.1 to 1 eV, greater than the thermal potential. The exciton can move to the near molecules thanks to Forster or Dexter energy transfer, generally for diffusion lengths of about 10nm. In this cell the exciton can be separated only by the electrostatic energy of the electric field: considering the exciton as a dipole of length d and momentum $p = qd$, the energy of its bond is given by

$$U = \frac{q^2}{4\pi\varepsilon d} \approx 0.5eV$$

It is thus necessary that the energy of the electric field is greater than U to separate the exciton, so

$$E \geq \frac{U}{p} \approx 4.8\frac{MV}{cm}$$

The intrinsic electric field of a single layer cell, however, is proportional to the difference in the work function of the electrodes. Considering a common value of 1eV and a width of the semiconductor film $t = 100nm$, the electric field would only be

$$E = \frac{\phi_A - \phi_K}{t} = 100\frac{KV}{cm}$$

thus the exciton cannot be separated by the energy of the intrinsic thermal potential alone, and no charge carriers are collected into the electrodes.

3.0.1 Double layer solar cells

The semiconductor film of these cells is composed by two different layers, a p-type whose HOMO band is aligned with the anode and a n-type whose LUMO band is aligned with the cathode, thus realizing two ohmic contacts.

The interface between the two layers shows a discontinuity in the energy bands which can be seen as a delta in the electric field, therefore leading to the separation of the excitons that are created within a distance from the interface equals to their diffusion length. An *active layer* can be defined as the region of the semiconductor in which the creation of an exciton leads to an effective separation of the charge carriers. The width of this active layer is twice the diffusion length.

3.0.2 Bulk heterojunction solar cells

To overcome the limits of the active layer, the double layer structure is evolved in an *interdigitated structure*. The semiconductor layers become comb-like structures, close

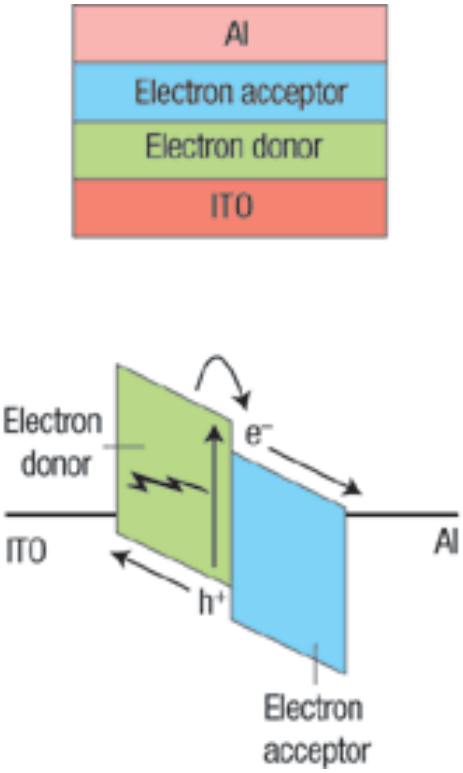

Figure 3.2: Double layer organic solar cell.

together. This way the interface area largely increases, ant the probability for an exciton that is created in a random point of the semiconductor to be near enough to the interface and separated strongly increases.

The realization of an interdigitated structure, though, is very complex since an high precision is required to correctly deposit the fingers. A different and less expensive approach have thus been developed to obtain the *bulk heterojunction solar cells*.

The essence of the bulk heterojunction is basically the same as the interdigitated structure, but the semiconductors are mixed together into a blend, as seen in fig. 3.3. If a path exist between the interface and the contacts, then the two separated charge carriers can be successfully collected and they contribute to the current delivered by the solar cells. The main challenge is to control the mixture of the layers in order to avoid the formation of isolated regions: these regions don't contribute to the generation of polarons, since a carrier generate inside one of these "islands" won't find a path to its electrode and will eventually recombine with another carrier.

3.0.3 Electric Model

The electric model of an organic solar cell must account for:

- the photogenerated current
- the recombination current inside the cell.
- the diode behavior under dark

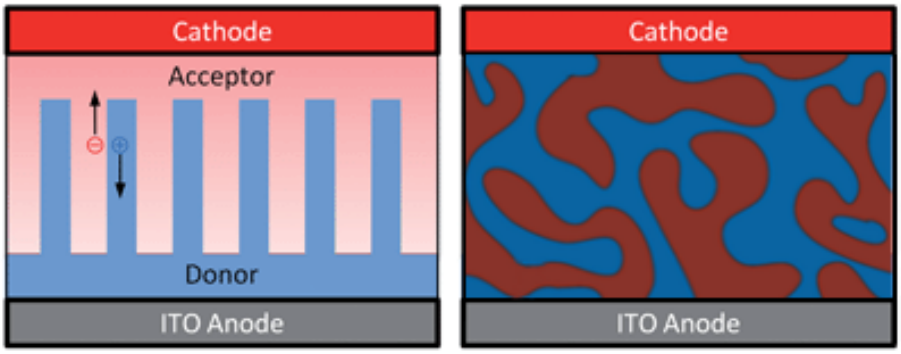

(a)

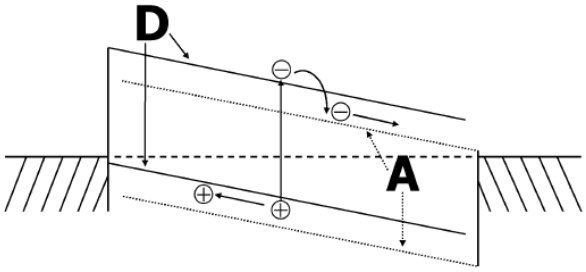

(b)

Figure 3.3: (a) Interdigitated structure (left) and bulk heterojunction (right). (b) The band diagram shows that there's a smaller effective band gap inside the blend.

- the effects of the shunt, that are small conductive parasite paths that connects the electrodes, that appear during the manufacture process.
- the contact resistance

The photogenerated current, as stated before, is proportional to the charge carriers that are generated with the absorption of the incident photons and successfully collected at the electrodes, so in the model it can be represented as a light controlled current generator. The recombination current is a inner current that represent those charge carriers which recombine instead of reaching the contacts. It has been found that this current is proportional to the applied voltage, so it is represented in the model as a voltage dependent current generator with opposite direction in respect to the previous generator. When the cell is under dark conditions the current generator doesn't dispense current, and the cell work as a diode, with a current

$$I_D = J_0 \left(\frac{V_D - V_{ON}}{V_0} \right)^{\nu} \qquad if V > V_{ON}$$

The effect of the shunts and the contact resistance are represented as resistors, one in parallel for the shunts (the more shunt there are, the less resistance it oppose) and one in series for the contacts. The resulting circuit is shown in figure 3.4.

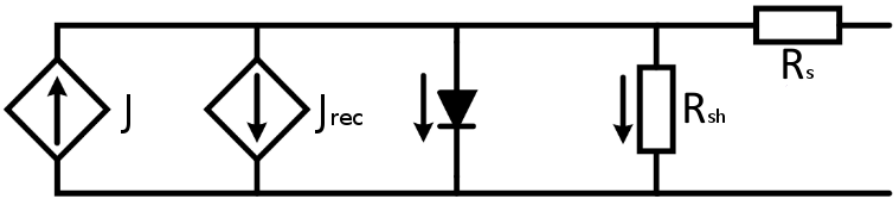

Figure 3.4: Electric model of the organic solar cells

Chapter 4

Instrumentation and measurements

This thesis focus on the effects of electric and thermal stresses on bulk-heterojunction polymeric solar cells based on P3HT:PCBM, fabricated at the Danmarks Tekniske Universitet. The structure of each cell is shown in fig. 4.1 on the following page: the first layer is the *Flextrode*, that is a flexible thin film made by a PET substrate, a silver grid, and a PEDOT:PSS layer and a ZnO layer to obtain a good band alignment. In contrast to the widely used but costly ITO electrodes, it exist in several versions that employ little or no scarce elements, and is processed in the ambient atmosphere by energy- and cost-effective roll-to-roll processing known from mass production. On the Flextrode is deposed the active layer, a P3HT:PCBM blend in which the former is a p-type semiconductor and the latter is a n-type. The PEDOT:PSS is a transparent, conductive polymer used as a electrode. On top of that another silver grid is deposed, and finally the cell is encapsulated to protect it from the effect of the air moisture, which has proven to be a crucial degradation factor in organic electronics.

The work begins with a first characterization of the solar cells. A complete characterization include the Isc, Voc and IV measurements, an Impedance Spectroscopy and the analysis of the Quantic Efficiency. Following is a brief explanation of the equipment used:

- The **E5263A High Speed Source Monitor** (Agilent Technologies) is an electronic instrument for the semiconductor DC parametric measurement. It provides several functions, such as sweep output, pulse output, and trigger functions, in the GPIB remote conditions. It has been used for measuring the Isc and a Voc of the solar cells, and for the voltage sweep to obtain the IV curve.

- The **SI1260 Impedance/Gain-Phase Analyzer** provides a comprehensive range of impedance and frequency response measuring facilities. In particular it has been used to measure the impedance of the cells while varying the frequency from an order of magnitude of tens of hertz to the megahertz.

- The **LOANA Solar cells analysis system** combines various measurement methods in one machine in order to analyze silicon solar cells. It has provided measures of the external quantum efficiency as a function of the light wavelength.

To connect the cell to the measurement system the sample holder (fig. 4.3) has

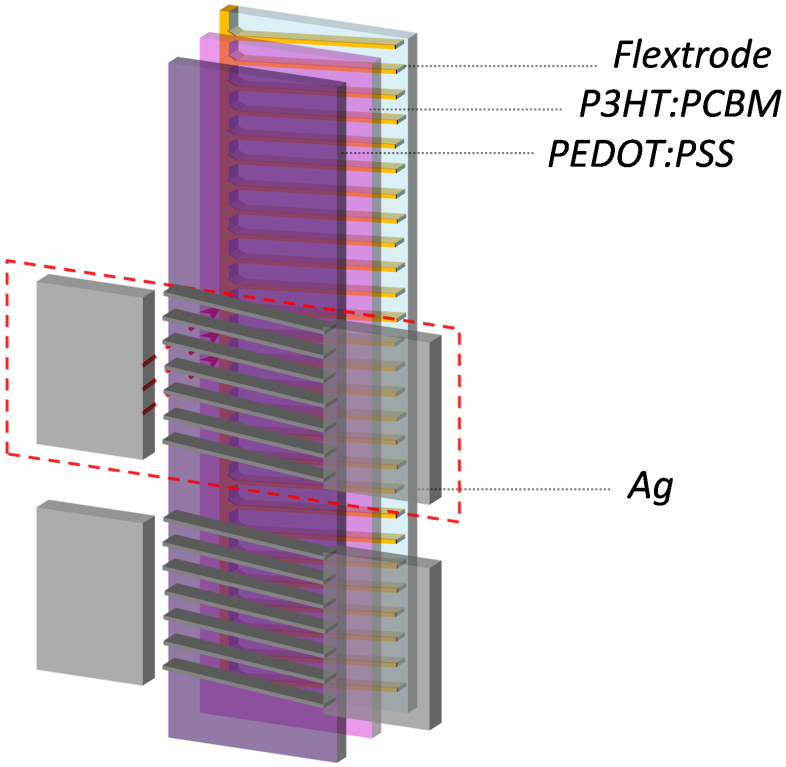

Figure 4.1: Structure of a DTU polymeric solar cell

Figure 4.2: The SI1260 (above) and the E5263A (below). The instrument are connected to the cell through a switching matrix, to automate the process

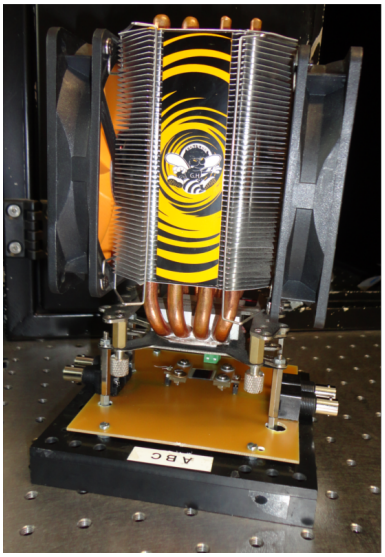

Figure 4.3: The sample holder placed underneath the LED illuminator.

been put underneath a white LED illuminator which provides a light intensity of 1 Sun[1] ($100mW/cm^2$), and inside a metal box that prevents external light from disturbing the measuring process.

[1]Calibrated by means of a reference solar cell

4.0.4 IV characterizations

The solar cells that were sent by DTU exhibit an active area of $1cm^2$, and differ by the depth of the active layer. In particular they are suddivided in three groups:

- 500nm active layer
- 300nm active layer
- 315nm active layer

It has been found that there aren't significant differences between in the IV curves of each group: even within the same category of cells the characteristics show a certain variability, and the ranges in which the parameters of each set of cells fluctuate overlap. This variability is very likely to be due to the manufacturing process of the samples not being fully automatized, and it is not an obstacle to the study of the effects of the stress. Fig. 4.4 shows two generic IV curves, one for the 500nm set and the other for the 315nm. As mentioned above they are similar, and the difference in short circuit current (Isc) and open circuit voltage (Voc) is within normal values.

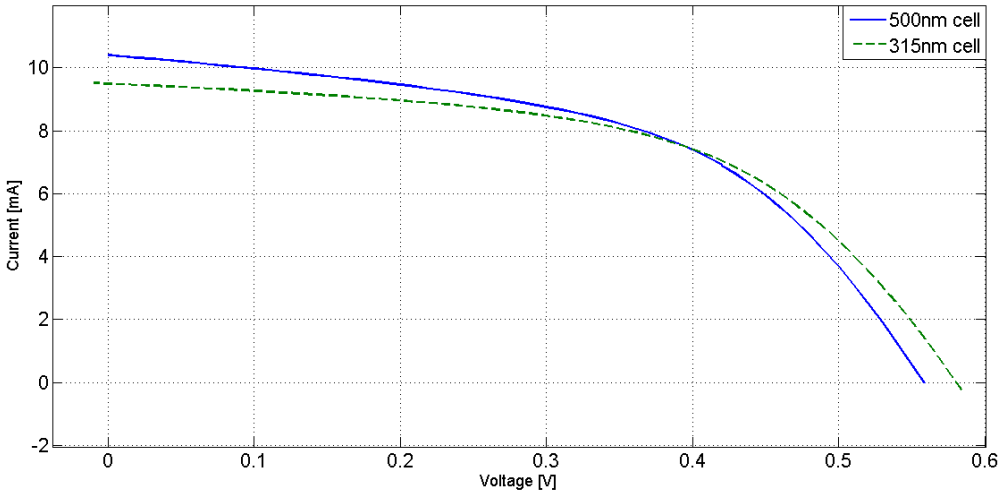

Figure 4.4: IV curves of a 500nm cell (solid line) and a 315 nm cell (dotted line). Differences depend on the not fully automatized manufacturing process, more than on the thickness of the active layer.

It is interesting to note that at low voltages the curves are not horizontal (as the one of an ideal solar cell would be), but show a slope which also varies from cell to cell. This slope is probably due to *shunts*: during the deposition process, small high-conductive paths can form between the silver fingers on each side of the cell. These paths are in fact the short circuits modeled as a parallel *shunt resistance* (R_{sh}) in the electric model of the polymeric solar cells, which is inversely proportional to the slope. The effects of the shunts also affects the current flowing in inversion conditions, as shown in fig. 4.5 where even at low inverse voltages the current reaches values of over 1mA.

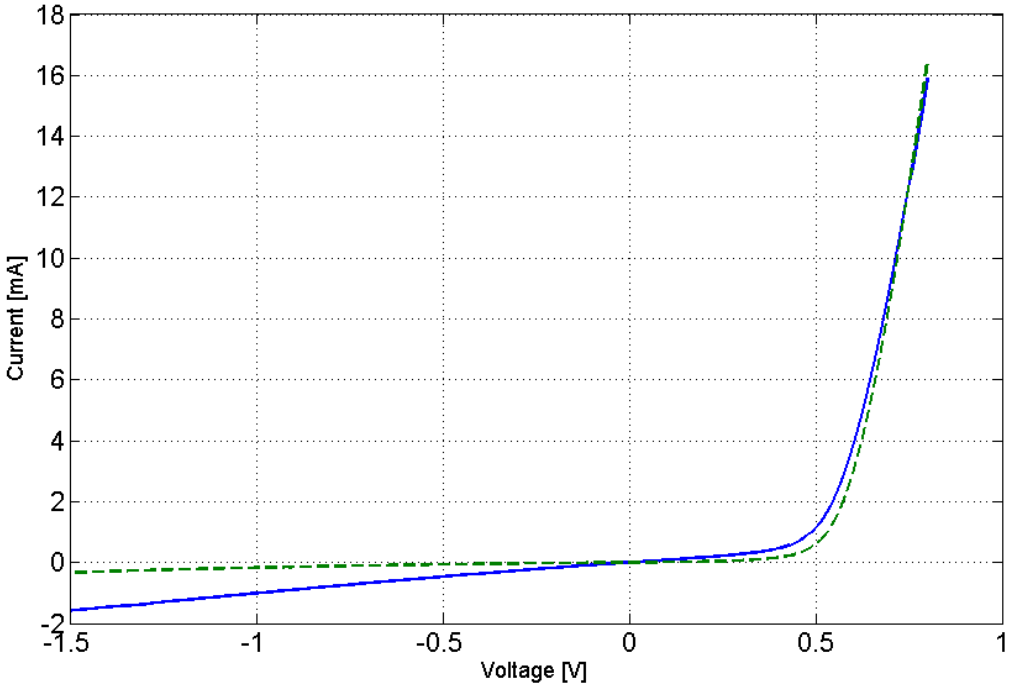

Figure 4.5: Effect of shunts in the inverse current of the cells. The slope of the solid line is rather pronounced, leading to current values of about 2mA when an inverse voltage of 1.5V is applied.

Figures of Merit

In table 4.2 are listed the figures of merit of each cell, subdivided by thickness of the active layer. Again a certain fluctuation is present, as expected; In figg. 4.6, 4.7, 4.8, 4.9 these variations are illustrated with Weibull Plots. The *fill factor* of the measured cells hardly exceed 50%, and remains in the range of $40-50\%$ instead. This means that the cells are quite far from the ideal solar cell, as the supplied current decreases considerably even when the voltage is lower than Voc. The *electric efficiency* η is proportional to the fill factor, and ranges between $2-3\%$. This could be seen as a poor performance, considering that the efficiency of inorganic solar cells can exceed 25%. However, considering the difficulties in the fabrication process of the test samples and the fact that currently organic solar cells exhibit lower efficiencies than their inorganic counterpart, it is a low but acceptable value.

Set	Isc $[mA]$	Voc $[V]$	$Pmax$ $[mW]$	FF [%]	η [%]
500nm	$10,43$	$0,56$	$2,82$	$48,32$	$2,82$
300nm	$11,27$	$0,56$	$3,12$	$49,04$	$3,12$
315nm	$9,48$	$0,57$	$2,27$	$42,7$	$2,27$
Total	$10,39$	$0,56$	$2,74$	$46,69$	$2,74$

Table 4.1: Mean values of the figures of merit of each set and of the totality of the cells.

Isc $[mA]$	Voc $[V]$	$Pmax$ $[mW]$	FF [%]	η [%]	Set
10.04	0.554	2.7	48.55	2.7	
9.68	0.561	2.61	47.99	2.61	
10.06	0.558	2.65	47.19	2.65	
10.95	0.563	2.95	47.76	2.95	
10.79	0.561	2.42	39.96	2.42	500nm
10.34	0.558	2.92	50.66	2.92	
11.63	0.565	3.26	49.65	3.26	
10.92	0.559	3.07	50.29	3.07	
10.33	0.557	2.95	51.33	2.95	
9.52	0.555	2.63	49.77	2.63	
11.27	0.56	3.08	48.77	3.08	
11.14	0.564	3.33	53.03	3.33	
10.74	0.569	3.13	51.28	3.13	300nm
11.8	0.576	3.26	47.91	3.26	
12.07	0.557	3.03	45.06	3.03	
10.61	0.56	2.86	48.17	2.86	
6.93	0.562	1.63	41.89	1.63	
9.51	0.581	2.98	53.92	2.98	
8.45	0.559	2.11	44.65	2.11	
8.66	0.561	2.02	41.56	2.02	
7	0.597	1.7	40.75	1.7	
8.03	0.593	2.06	43.25	2.06	315nm
9.93	0.582	2.67	46.27	2.67	
11.29	0.546	2.44	39.53	2.44	
11.9	0.542	2.4	37.22	2.4	
13.12	0.538	2.68	37.97	2.68	

Table 4.2: Figures of merit of the measured samples, subdivided by thickness of the active layer. On top are the 500nm cells, in the middle the 300nm cells and on the bottom the 315nm cells.

4.0.5 Impedance Spectroscopy

Impedance Spectroscopy (IS) has become a major tool for investigating the properties of the solar cells. It is measured by applying an AC potential to the cell, changing its frequency to cover the desired range and measuring the current that pass through. The applied potential is a small sinusoidal excitation signal, to keep the cell's response pseudo-linear. For the same reason a bias can be applied, to force the more suitable operating point.

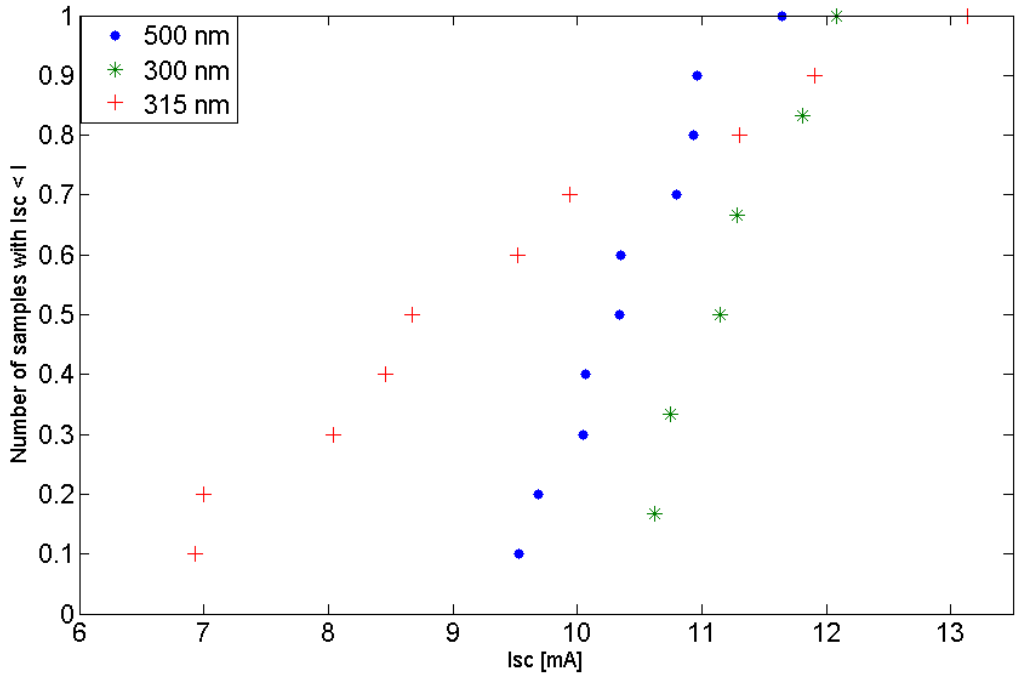

Figure 4.6

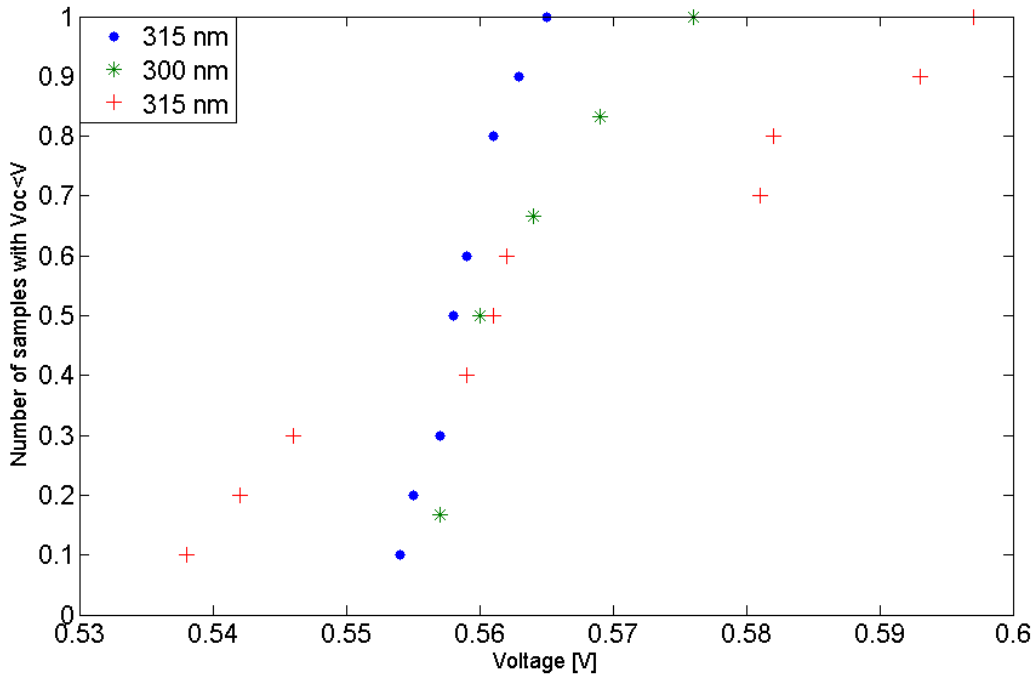

Figure 4.7

The impedance is calculated by

$$Z = \frac{E_t}{I_t} = \frac{E_0}{I_0} e^{i\omega t}$$

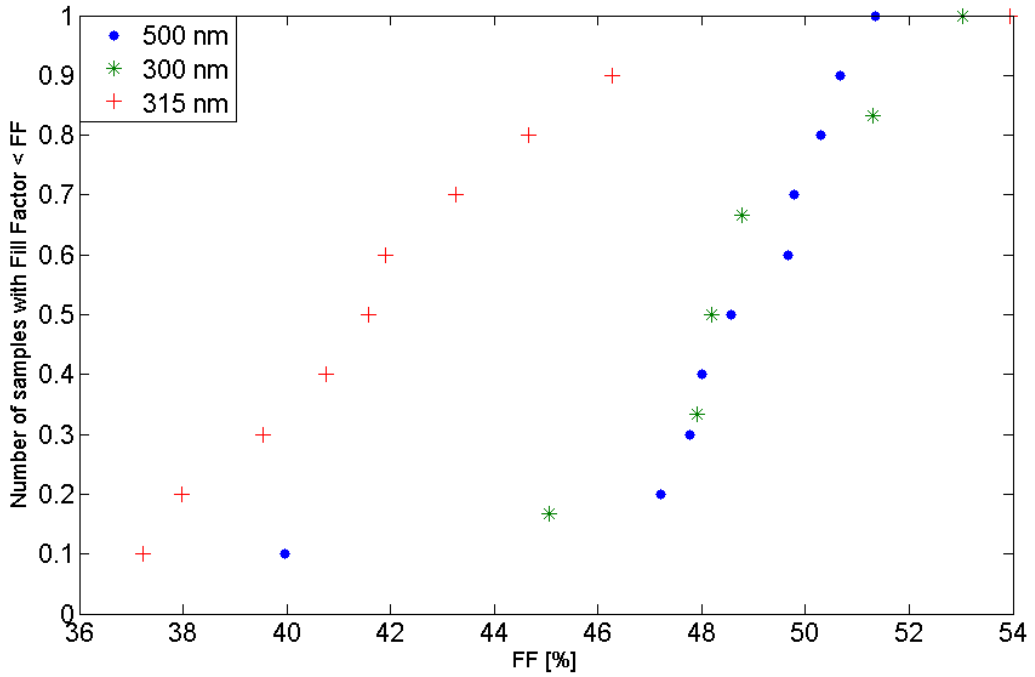

Figure 4.8

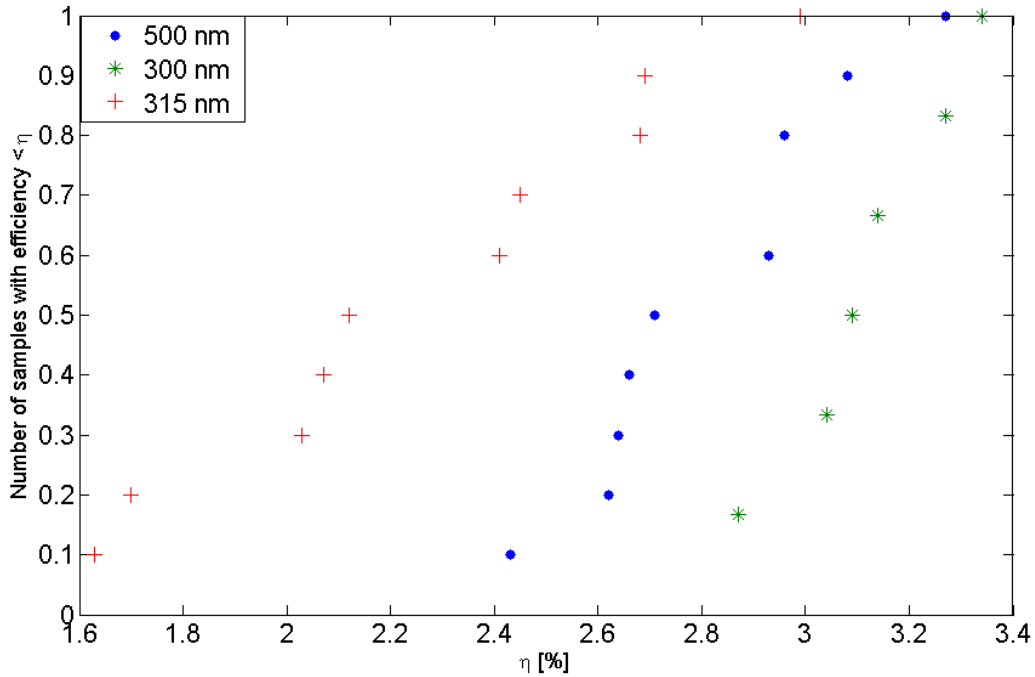

Figure 4.9

which is the sum of a magnitude Z_o and a phase shift ϕ. If the real part is plotted on the X-axis and the imaginary part is plotted on the Y-axis of a chart, we get a *Nyquist Plot*. The Nyquist plot of the impedance of a simple RC circuit is shown in fig 4.10 on the following page: it is a single semicircle (*lobe*). Each point on the Nyquist Plot is the

impedance at one frequency.

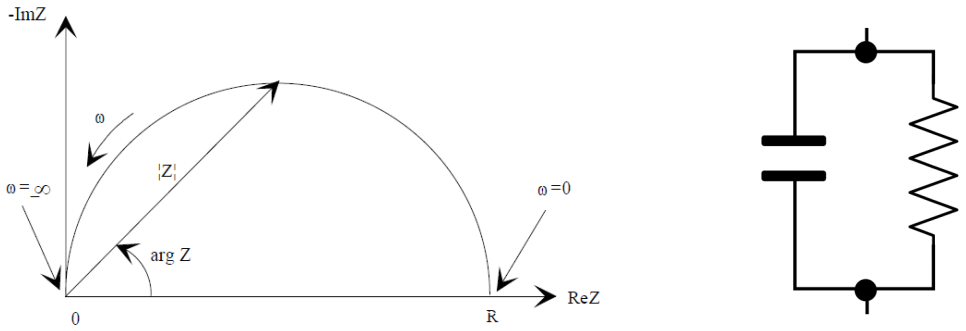

Figure 4.10: The Nyquist Plot (left) of a simple RC circuit (right). The plot is a semicircle (a lobe) which tends to the origin at high frequencies.

The data from an impedance spectroscopy can be used to obtain a model of the impedance of the cell, with some reverse engineering. Considering fig. 4.10, the cutoff frequency of the corresponding circuit can be estimated plotting the imaginary part as a function of the frequency and locating the peak of the curve, while the resistance value is approximately the diameter of the lobe. The capacitor's value can thus be easily calculated by

$$C = \frac{1}{2\pi f R}$$

The electric models of more complex Nyquist Plots are a combination of common electrical elements such as resistors, capacitors, and inductors. To be useful, the elements in the model should represent a specific point in the cell. As an example, the cell's contact resistance can be modeled as a series resistance.

Following is the impedance spectroscopy of one of the studied samples, measured on a frequency range between 100Hz and 2MHz and biased to $V = Voc$. Two lobes can clearly be distinguished, and from fig. 4.12 the peak frequencies can be spotted. These lobes are not simply a series of two RC circuits, since their diameter and height don't fit to that simple model.

To extrapolate a correct model for the solar cells a series of impedance spectroscopies were conducted varying the light intensity and the bias and monitoring the changes in the impedance. For each intensity value from 0 to 1 Sun with steps of 0.1 Sun, the impedance was measured with -1.5V, -1V, -0.5V, 0V, 0.5V and Voc bias. An example can be seen in fig. 4.14. From the results two possible models have been found. The first model is the one shown in fig. 4.15, composed by two parallel RC and a distributed RC. Subtracting the two visible lobes a third hidden lobe has been found, thus the necessity of three RC circuits. In this case the high frequency lobe would be associated to one of the parallel RC and represents the interface between Zn and PEDOT. The low frequency lobe, which refers to the distributed RC, varies a lot when changing the light intensity and the bias, so it should model the impedance of the active layer. The hidden lobe would be a debye capacitance, caused by those electric charges that may be trapped at the interface with the contacts.

In the second model (fig. 4.16) the first module is composed by a distributed RC in series with a resistance, both in parallel with a capacitance. The second module is a

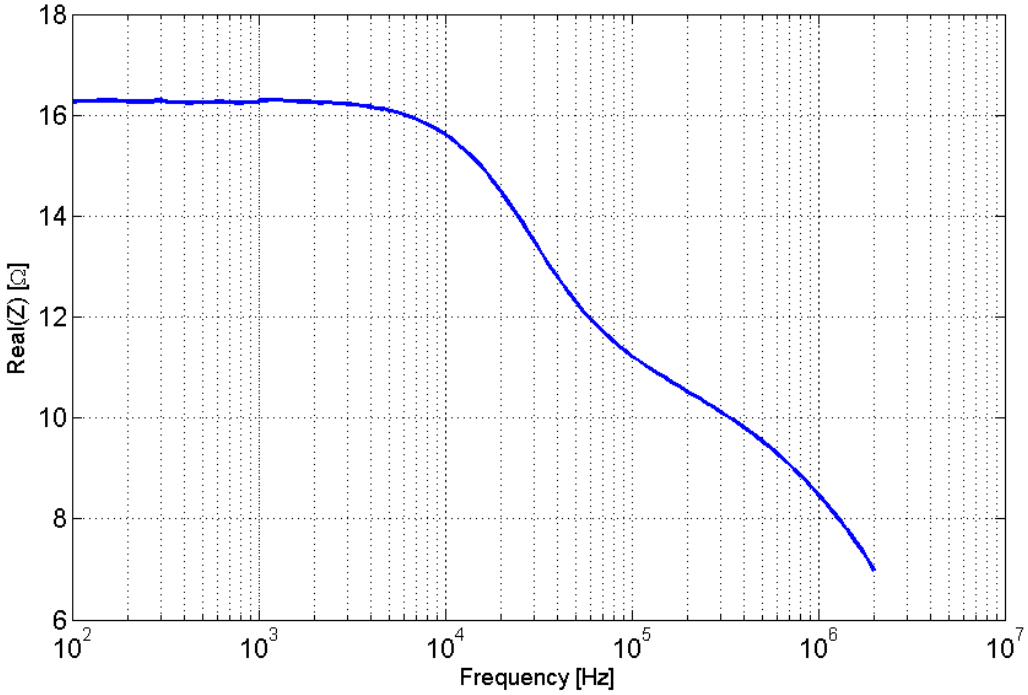

Figure 4.11: Real part of the measured impedance.

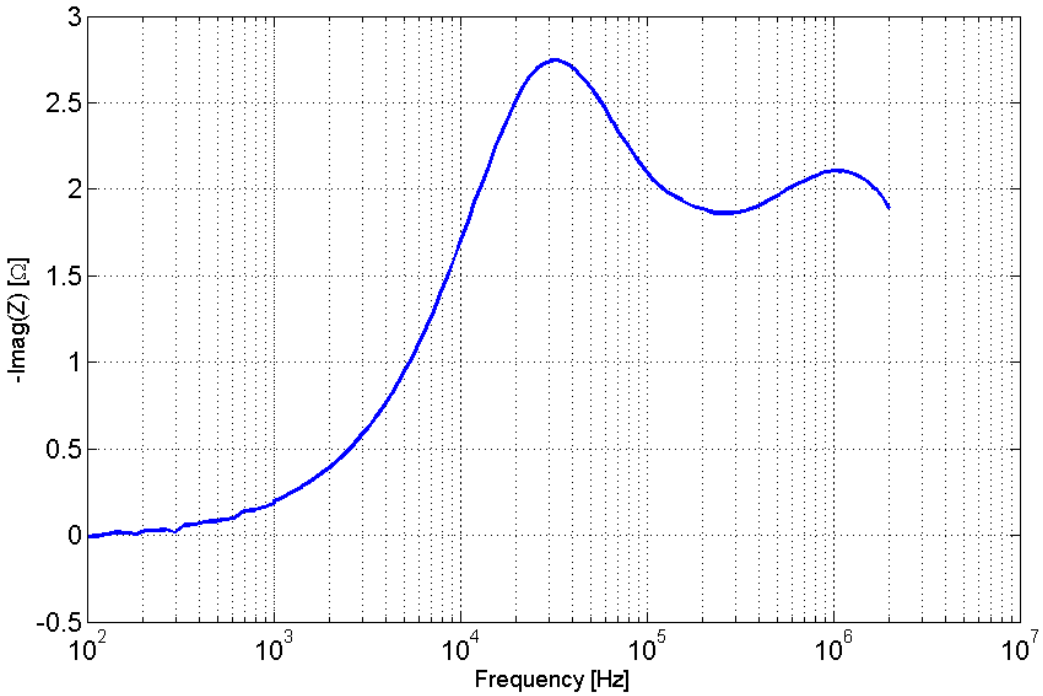

Figure 4.12: Imaginary part of the measured impedance.

distributed RC alone. Both modules refer the cell's blend, the first representing the the interface between Zn and PEDOT and the second the rest of the blend, for the same reason as the previous one. Both models have a series resistance which symbolize the

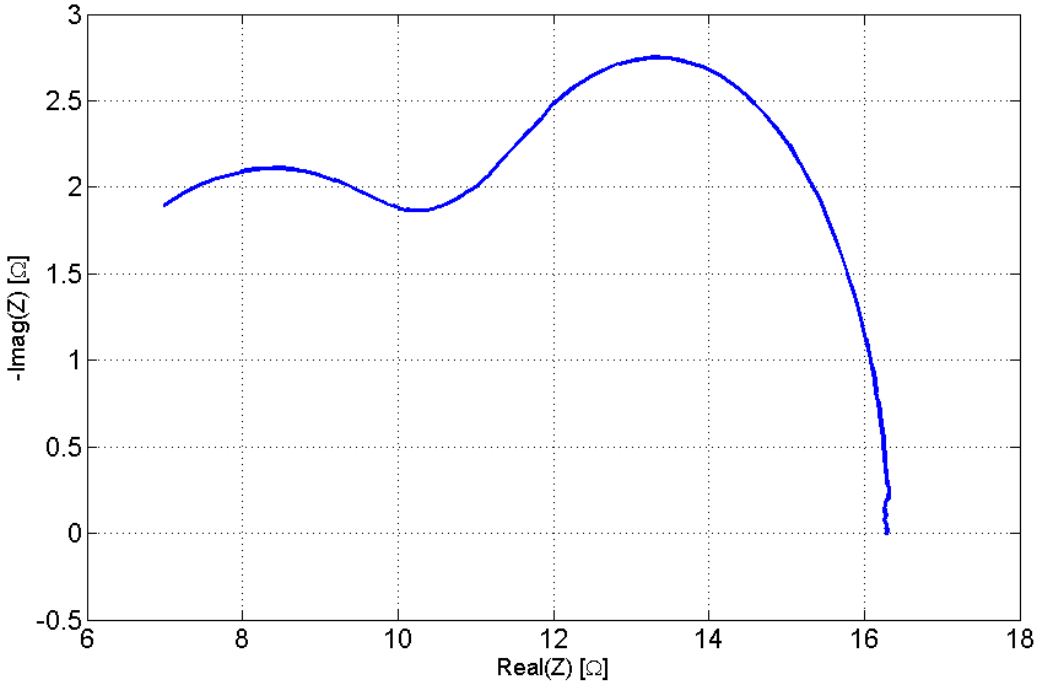

Figure 4.13: Nyquist plot of the measured impedance. Two lobes can be easily distinguished.

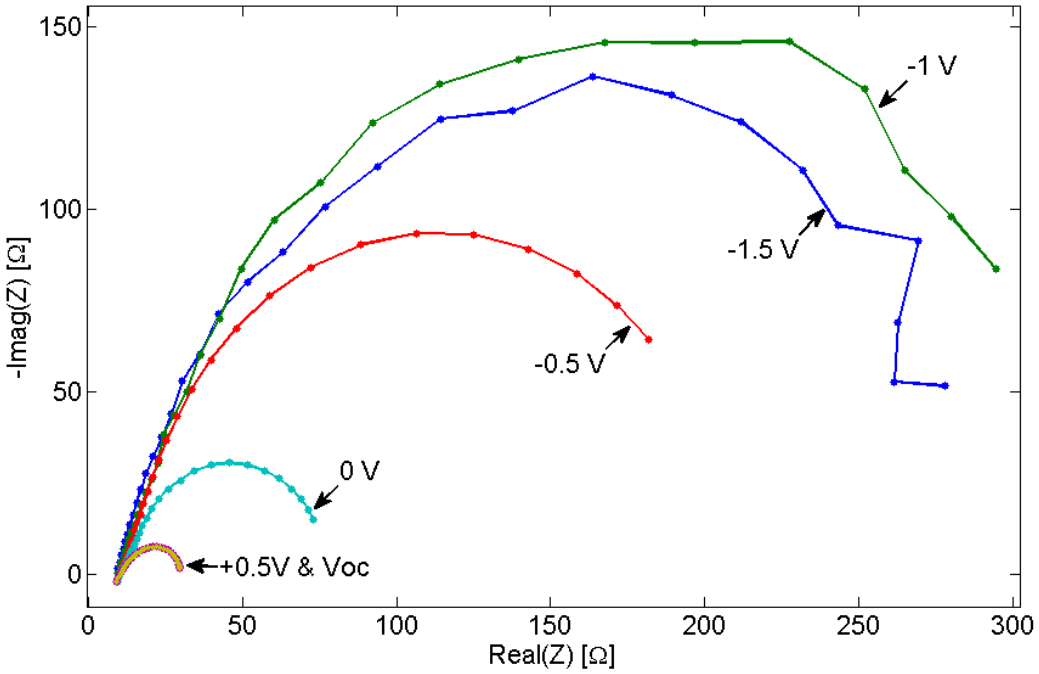

Figure 4.14: Impedance spectroscopies under 1 Sun, varying the bias from -1.5V to Voc.

contact resistance. The distributed RC is composed by an infinite series of the section shown in figure 4.17. A fitting of the first model is shown in figures 4.18 and 4.19 on page 46, on the impedance obtained under 1 Sun with a -0.5 V bias.

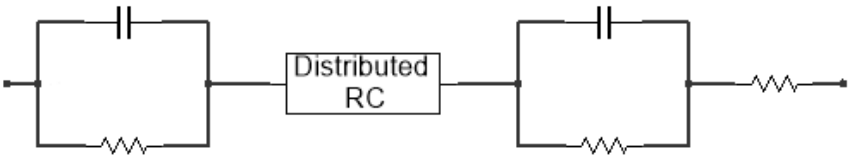

Figure 4.15: A model for the impedance of the solar cells

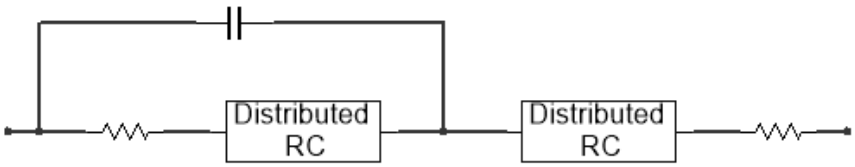

Figure 4.16: A model for the impedance of the solar cells

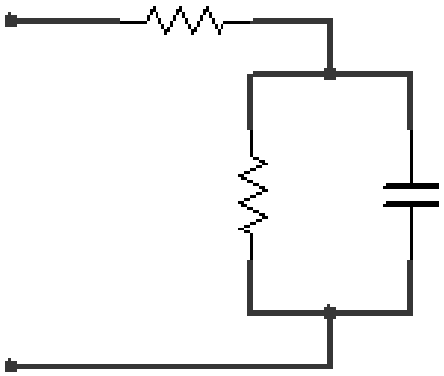

Figure 4.17: Infinitesimal section of the distributed RC

4.0.6 Efficiency

To end the characterization of the cells a measure of the external quantum efficiency was performed. The EQE is not a constant, its value is a function of the wavelength of the incident light since it depends on the absorption spectrum of the solar cell. The tested samples showed a quite identical behavior, even considering cells with different active layer thickness. Two examples are displayed in fig. 4.20 on page 47, and the other cells showed little alterations. The efficiency occupies the "violet side" of the visible spectrum, reaching its maximum at wavelengths of about 500nm and dropping to zero around 650nm.

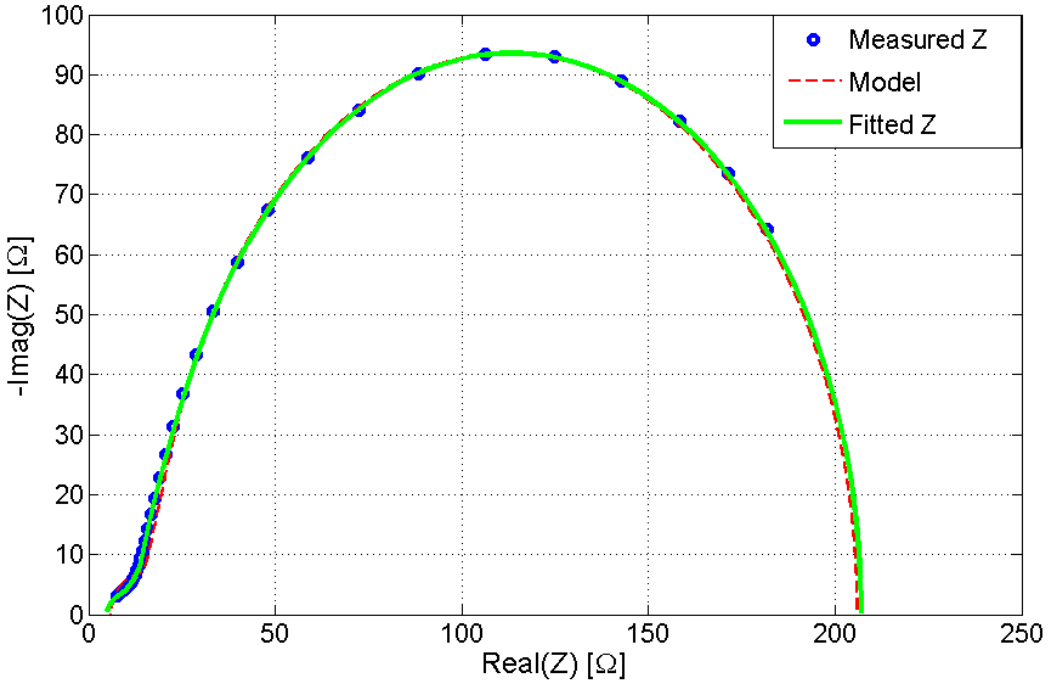

Figure 4.18: Fitting on the niquist plot of the impedance, using the model of figure 4.15

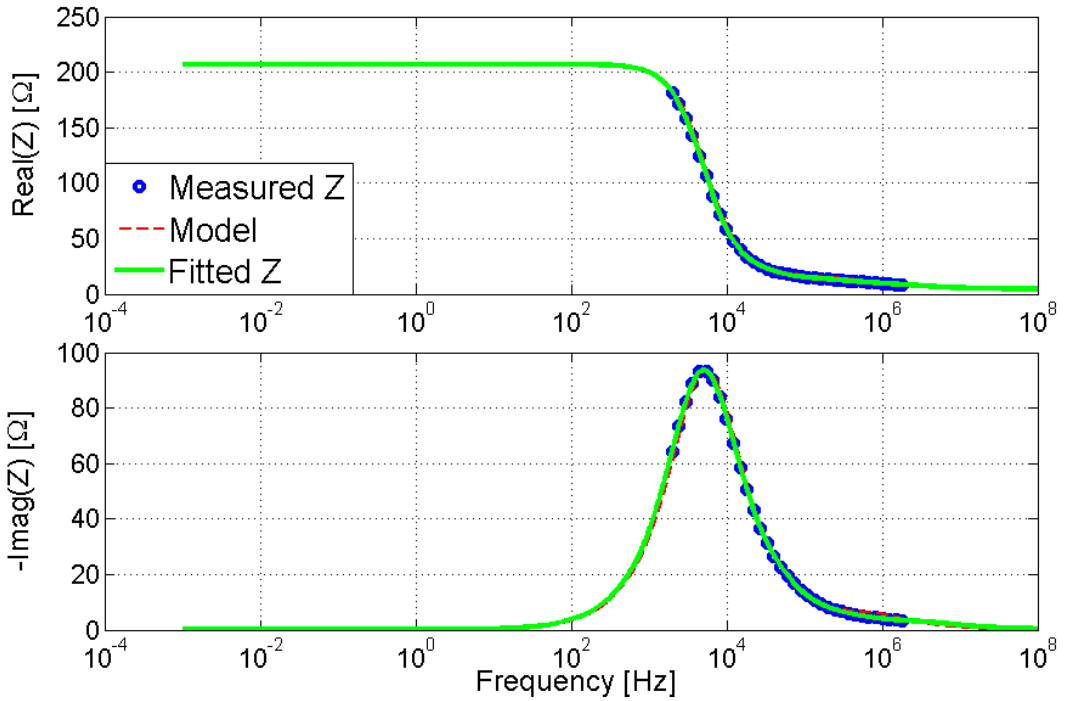

Figure 4.19: Fitting on the real and imaginary part of the empedance, using the model of figure 4.15

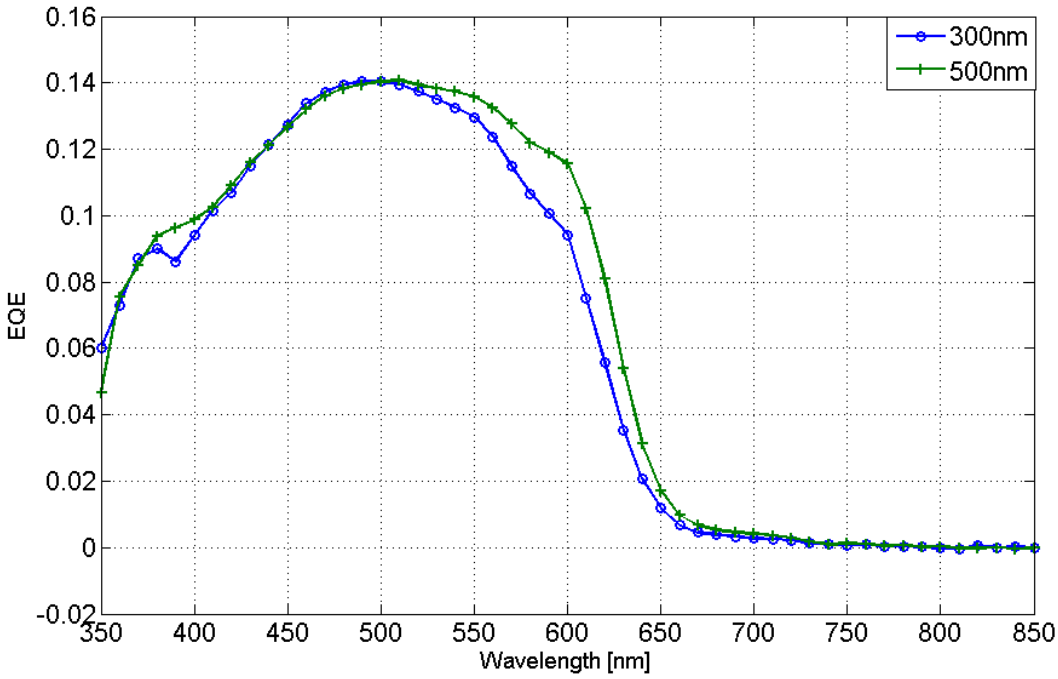

Figure 4.20: External quantum efficiency in function of the wavelength of the incident light. The 500nm and the 300nm cells showed a quite identical behavior

Chapter 5

Electric and thermal stresses

The solar cells underwent to three different stress typologies, which are

- Forward current stress
- Inverse voltage stress
- Thermal stress

The stress procedures start with a characterization of the fresh cell, followed by a sequence of stress steps of a certain duration and under dark conditions. The characterizations include the measure of Isc, Voc, I-V curves and the impedance spectroscopy. At the end of each step the cell is measured again to monitor the evolution of the degradation. The stresses continue either until the breakdown of the cell, until a noticeable degradation is reached or until a maximum stress time is passed. Electric stresses[1] follow two different procedures, that differ in the magnitude of the voltage/current applied. In the first phase (*staircase stress*) the stress time is fixed at a constant value of 1000 seconds (0.28 hours), while the current/voltage magnitude starts from a base value and is increased after each step. In the second phase (*constant stress*) the current/voltage is fixed and it is the step duration that is increased.

5.1 Staircase stress

The procedure of the staircase voltage stress begins by imposing an inverse voltage to the cell, starting with 2V and increasing by 0.2V after each step. The inverse current that flows during the stress is monitored, to have an idea of the power dissipation. The stressed cells underwent a monotonic degradation: fig. 5.1 on the following page displays the evolution of the I-V curves, which shift downwards until the breakdown. In particular it is interesting to note that while the Isc reduces remarkably, the Voc seems to be unaffected until the breakdown occurs. This could mean that the origin of the degradation is to be attributed to a decrease of the generation rate, either due to the formation of exciton quenching centres or to a growth of the recombination *inside* the active layer

[1] Current and voltage stresses

(thus preventing the charge carriers from reaching the cell's contacts). In fact the short circuits current can be expressed as following:

$$J_{sc} = qn_{e-h}\eta_e$$

where q is the electric charge, n_{e-h} is the number of electron-hole pairs generated per unit of incident solar energy, and η_e is the fraction of charge carriers that successfully reach the cell's contacts overcoming recombination. In fig. 5.2 on the next page the progression of the Isc of two stressed cells is detailed. The degradation is slow but constant, and last until the breakdown of the cell. In fig. 5.3 is reported the evolution of the figures of merit: as mentioned the Voc doesn't vary in a prominent way, while the efficiency follows the Isc trend. The fill factor of one of the cells shows an increment of about 5%, but it is only due to the fact that the Isc decreases greatly while Voc remains the same.

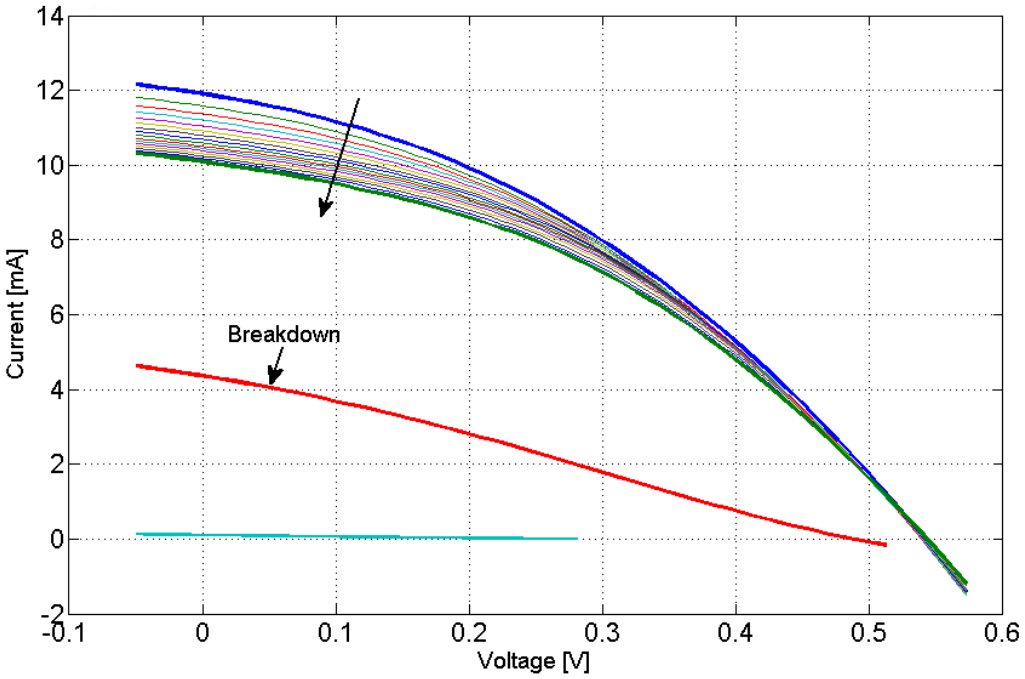

Figure 5.1: Evolution of the I-V curves of a 315nm cell during the staircase voltage stress. The monotonic degradation is specified by the arrow.

The impedance spectroscopy showed that the impedance of the cells didn't alter much. In fact the peak frequency of the lobes remains the same, and the more consistent variations are those of the real part of the impedance, which however increases by only a few ohms that contribute to the small lengthen of the lobes. When breakdown occurs, predictably, the impedance values increase of a few orders of magnitude (fig 5.4, 5.5 and 5.6).

The procedure of a staircase current stress consists in a first stress step conducted by imposing a current of 20mA to the cell, followed by a series of steps in which current is each time increased by 20mA. The stress goes on until breakdown.

The results are quite different from the previous stress. The trends of the Isc and the other figures of merit (fig. 5.7 on page 54 and 5.15 on page 60) clearly reveal an odd behavior in the degradation, that can be subdivided in three distinct phases:

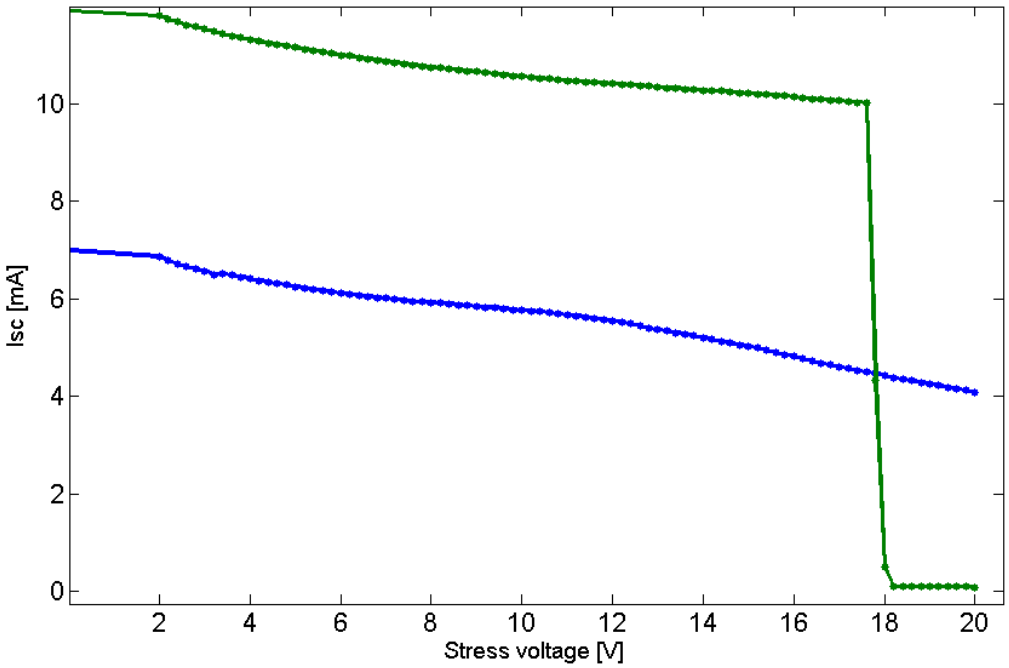

Figure 5.2: Degradation of the Isc of two 315nm cells. A cell reached breakdown just before 18V of inverse voltage, the other endured the stress with only a certain level of degradation.

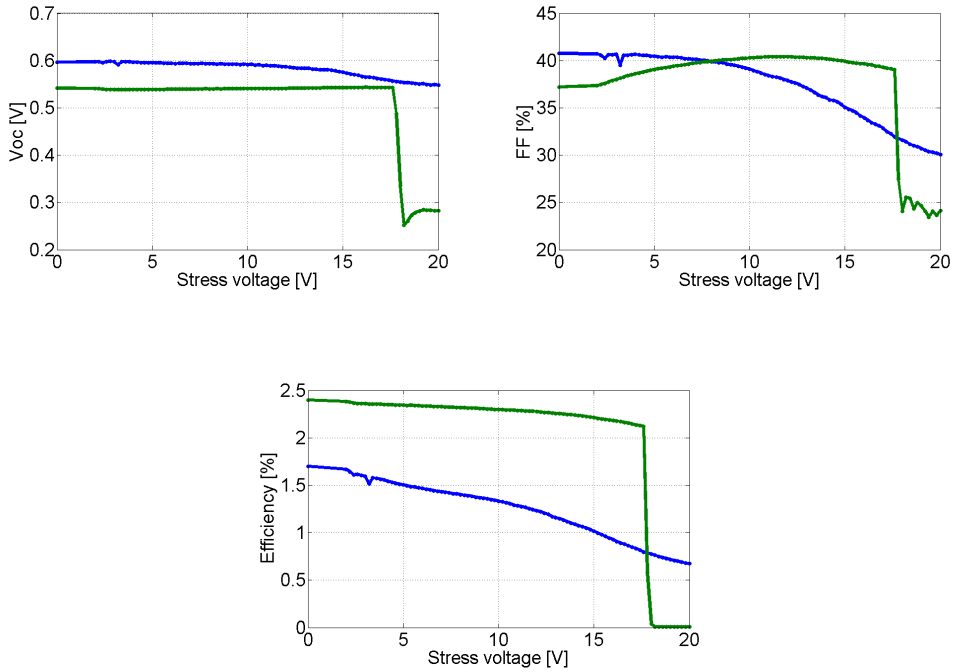

Figure 5.3: Evolution of the figures of merit of the voltage-stressed cells.

- In the first phase, which goes from the initial 20mA stress current to 180mA, the degradation appears to be the same that goes on during the voltage stress. The Isc decreases and the Voc show some variations, probably due to the progressive creation and cauterization of shunts (fig. 5.8 on page 54).

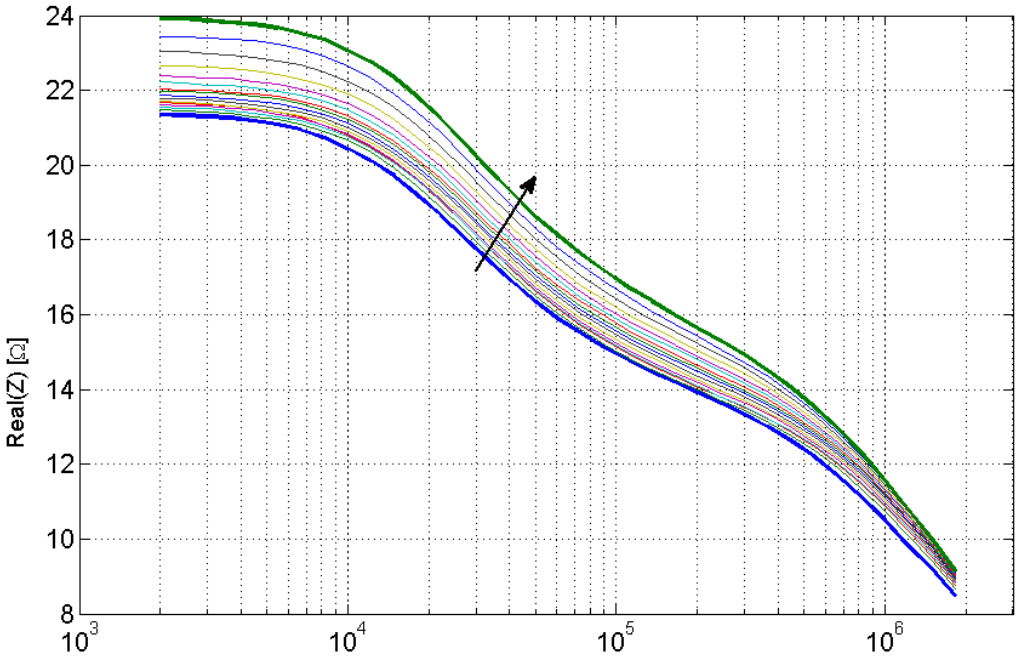

Figure 5.4: Real part of the impedance spectroscopy as the stress progressed, before breakdown.

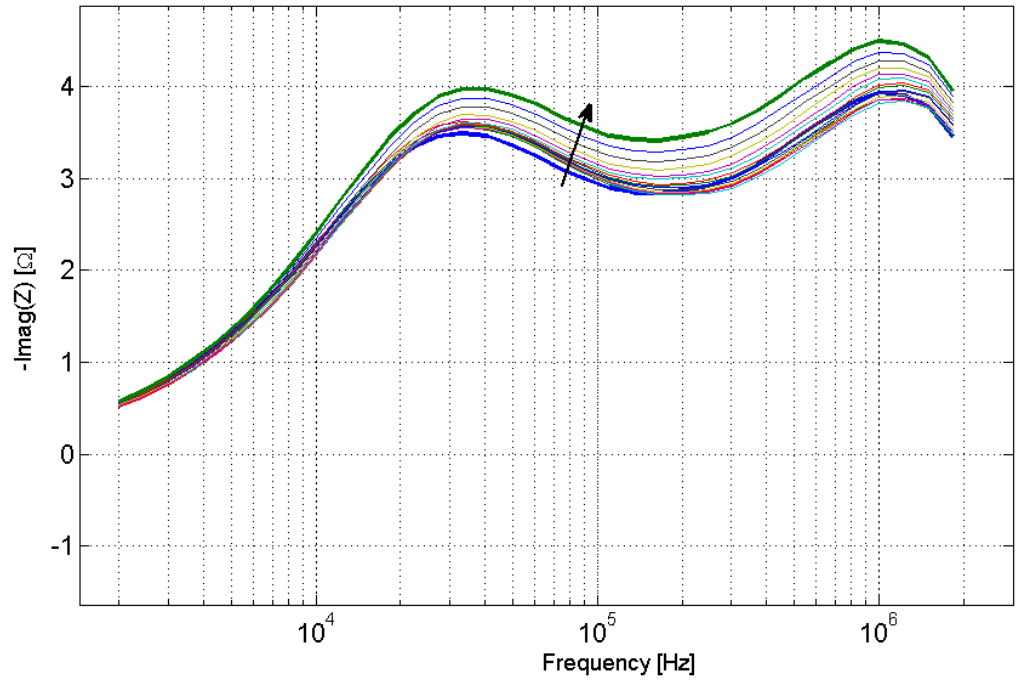

Figure 5.5: Imaginary part of the impedance spectroscopy as the stress progressed, before breakdown.

- The second phase is the most interesting one: here some kind of recovering seems to happen, as the Isc moves upward. The I-V curves start shifting upward too, and it should be noted that the slope of these curves decreases in respect to the curves

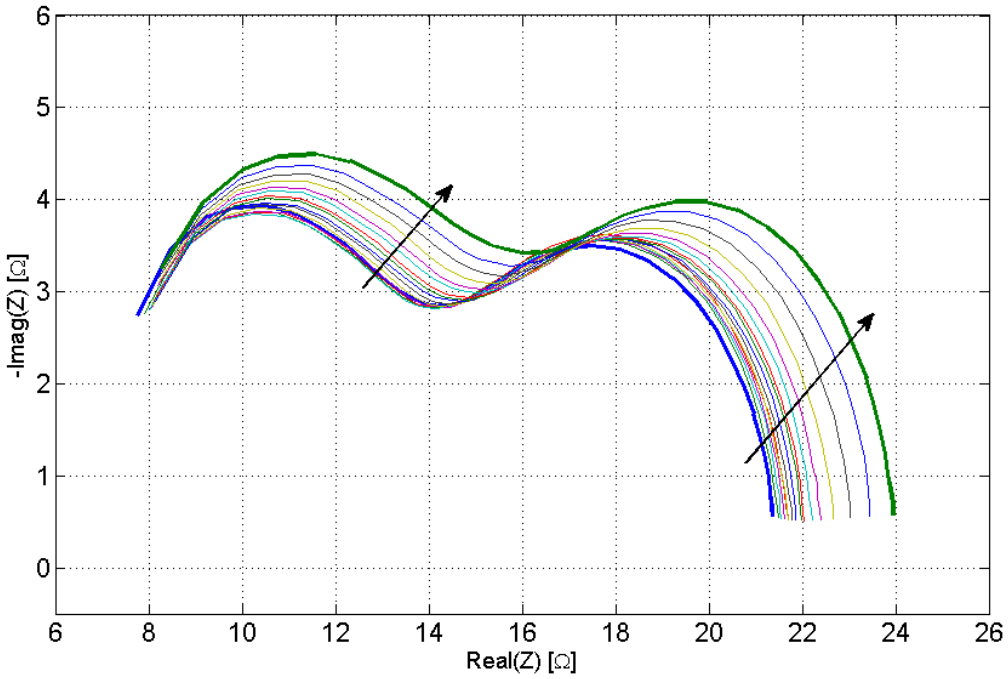

Figure 5.6: Nyquist plot of the impedance spectroscopy. Again two lobes can be distinguished.

from the previous phase, possibly indicating an increase of the shunt resistance due to the burnt of the shunts (fig. 5.9 on page 55).

- In the third phase the recover stops or, more likely, the degradation starts to prevail. The cell's performances drop again and keep this trend until the breakdown (fig. 5.10 on page 55).

The three phases can also be seen in the impedance spectroscopy, shown in fig. 5.16. It can be seen that while the high frequency lobe stays almost the same, the low frequency lobe (the one associated to the blend composing the active layer) increases greatly in the first phase with also a decreasing in its peak frequency, then goes back almost to normal at the end of the second phase, and restart increasing until breakdown in the third. This seems to confirm that the damage in the first phase indeed affects the active layer, as hypothesized before.

To explain the recovering that happens during the phase 2 of the current stress, the effect of the temperature has been considered. During the stress the power dissipation reached relatively high values, and considering the small dimensions of the samples this could have led to very high temperatures. The recovery could thus be associated with thermal annealing.

To prove this point, another cell was put under stress, but this time an infrared camera was used to monitor its temperature. Some specific current values were forced through the cell, while monitoring the voltage between cathode and anode to calculate the dissipated power. The results are shown in fig. 5.11 on page 56.

The cell reaches 100-120°C when the current is around 200-220mA. These results confirm the hypothesis of the thermal annealing: in phase 2 the temperature goes from

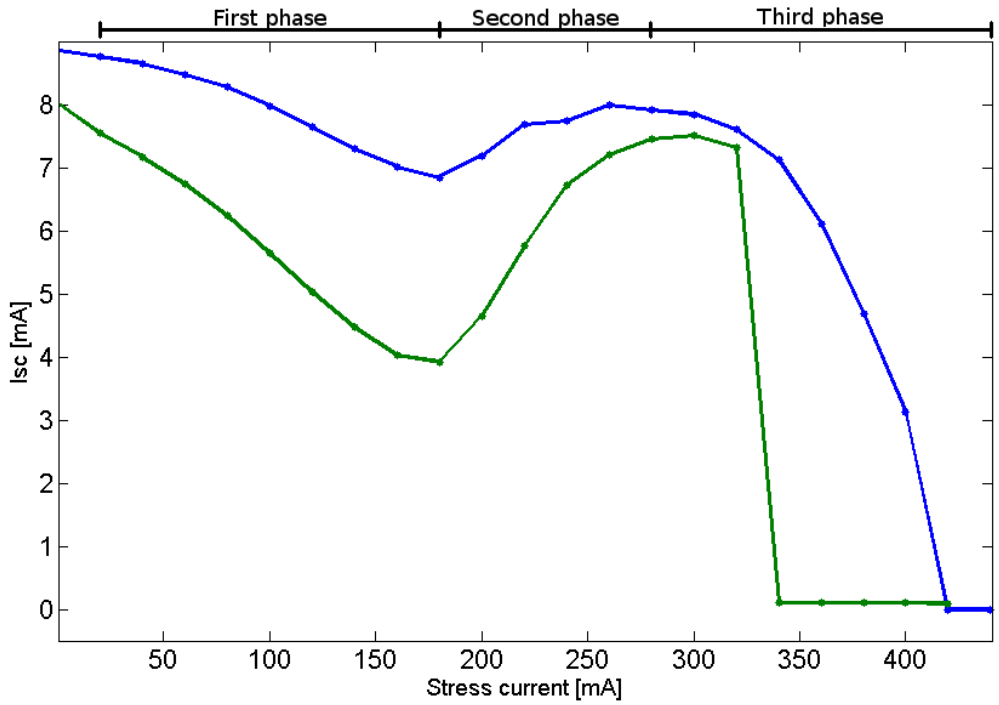

Figure 5.7: Isc kinetics of the two stressed cells, each one following the same behavior. In the first phase the degradation is similar to the one occurred during the voltage stress; in the second phase the Isc starts moving upward, suggesting a possible recover; in the third phase the recover stops, and the Isc drops down until the cell's breakdown.

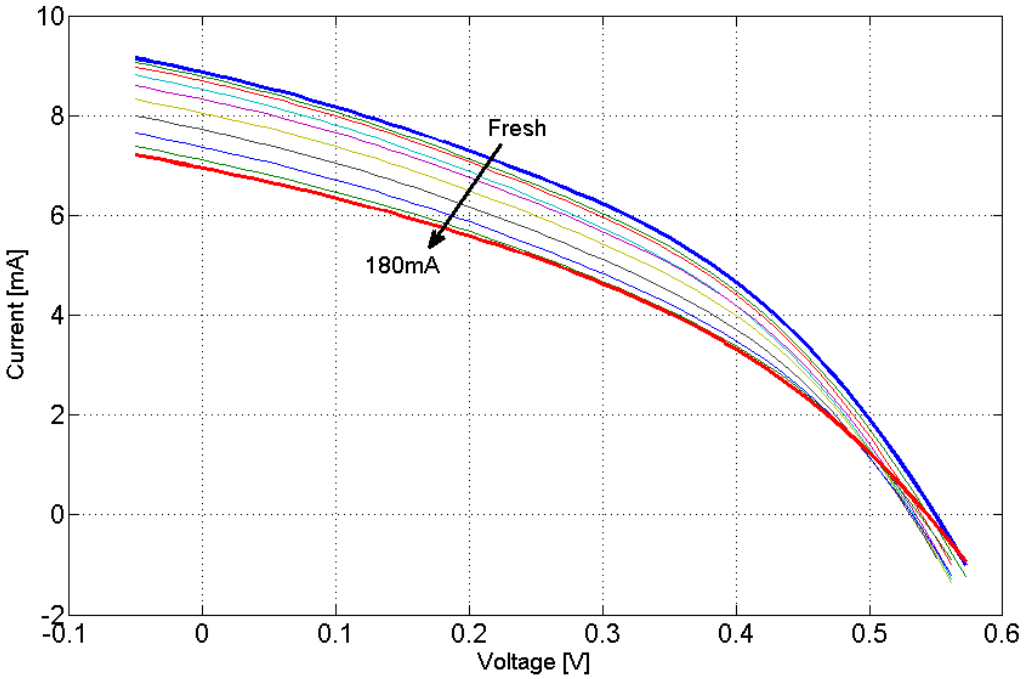

Figure 5.8: I-V curves, first phase. There is a clear degradation similar to the one occurred during the voltage stress.

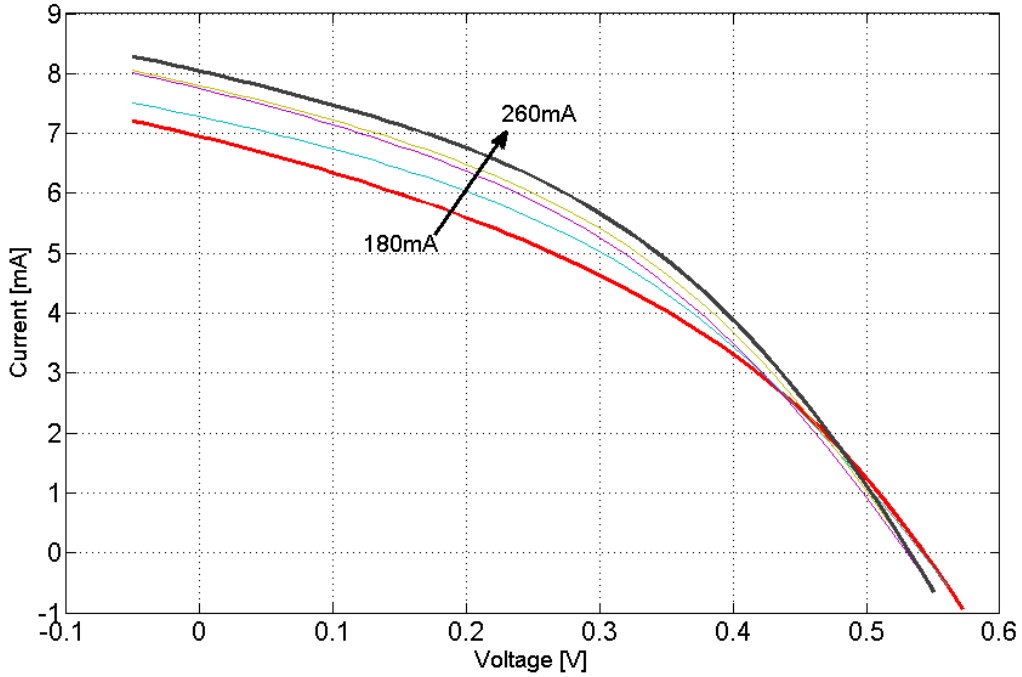

Figure 5.9: I-V curves, second phase. A recovery seems to happen, the curves shift upward and their slope decrease.

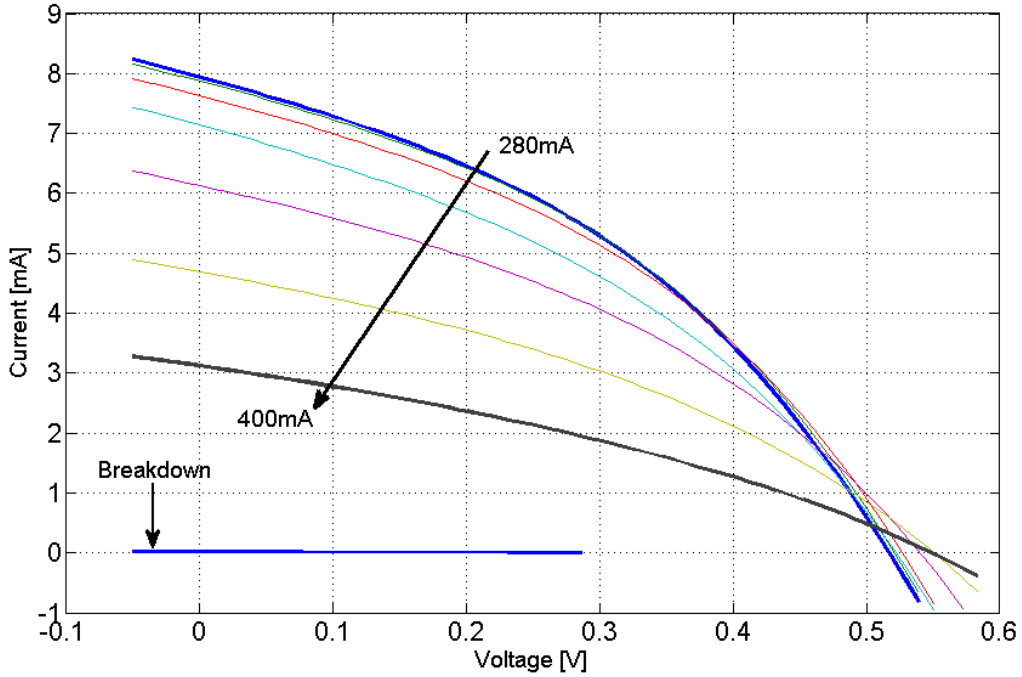

Figure 5.10: I-V curves, third phase. The downward shift recommence, and it goes on until breakdown.

90°C to 150°C, which are high enough to induce the annealing and thus the recovery of the cell but at the same time are low enough (or the 1000 seconds steps are short enough)

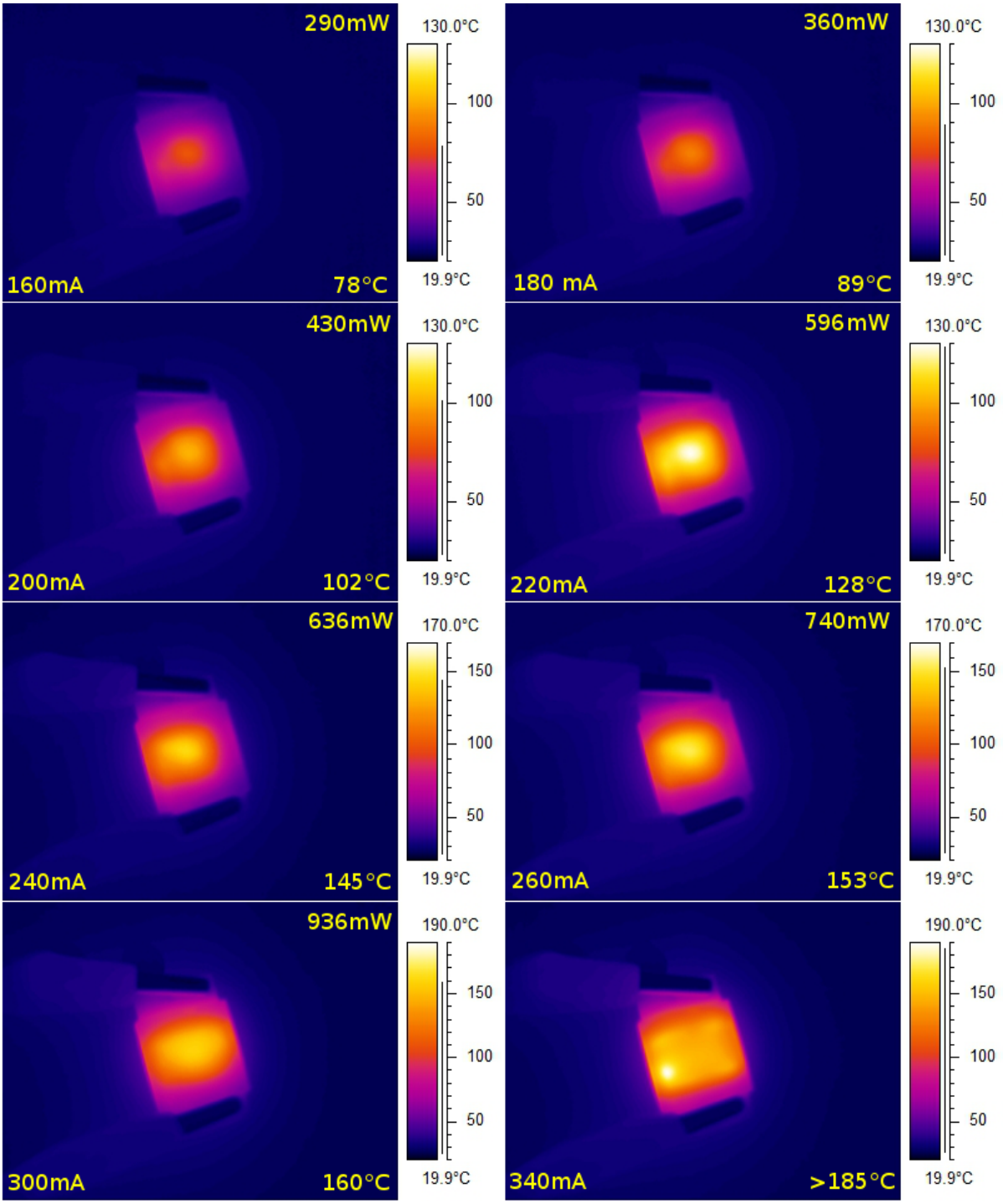

Figure 5.11: Pictures taken with the infrared camera on the cell put under current stress. Around 200-220mA the temperature reaches 100-120°C. In the last panel the picture was taken while the cell was breaking down, the temperature and the dissipated power were increasing rapidly.

to not cause the thermal degradation which occurs in phase 3. The stress current that flows during phase 2 still damages the cell, but this effect is dominated by the recovery, which prevails. When the stress current raise enough, though, its damage is *added* to the thermal damage induced by the higher temperatures and the degradation prevails

again. Furthermore, as mentioned before, during the second phase of the stress the IV curves show a reduction in their slope: it's worth noting that, while applying the 220mA current to the cell monitored by the infrared camera, the voltage between its contacts grew significantly over time (at the end it was about 20% higher than the starting value). This means that the slope of the IV curve decreased during the stress step, and can be explained with the progressive cauterization of the shunt channels.

To further prove the effect of the temperature on the stressed cells, the one sample that underwent the voltage stress but didn't reach breakdown was put into a controlled oven at 120°C for 1 hour, in dark conditions and unbiased[2]. As can be seen in fig. 5.12, and 5.13 on the following page, its performances improved considerably to the point that the Isc was even higher than the one of the fresh cell, probably because of the repair of some damage already present in the cell. The Voc, though, wasn't affected by the heating session as it stayed unaltered.

The one thing left to analyze is whether this recovery really brings back the cell to a "fresh" state, or if the annealed cell is just "patched" and less stable than a fresh one. The annealed cell has thus been stressed again, to see if its behavior was comparable to the first one. The results show that the cell is not stable as a fresh one. In fig. 5.14 on page 59 are the Isc kinetics of the cell, stressed before and after annealing. Even if the overall trend is the same, the Isc of the annealed cell shows some considerable drops which could be due to the creation of large shunts, meaning that the structure of the active layer is not the same as before the first stress. It's important to consider, however, that a thermal storage under 120°C for one hour could be too much by means of temperature or duration.

[2]In order to isolate the effects of temperature only.

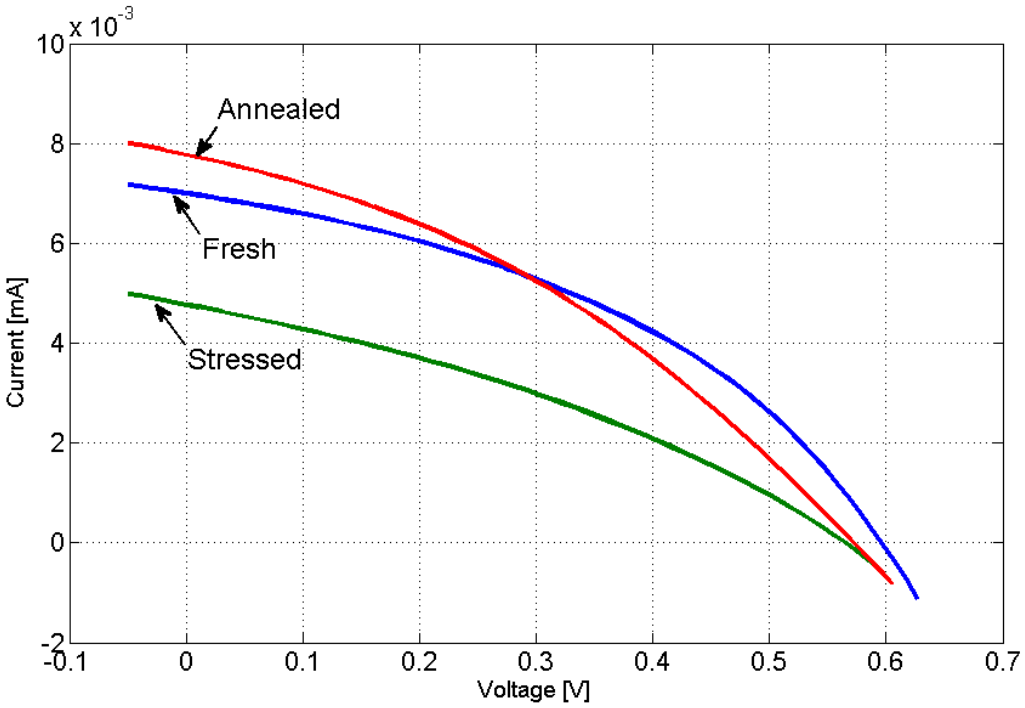

Figure 5.12: Effects of thermal annealing on a stressed cell. After 1 hour at 120°C the characteristics of the cell recovered.

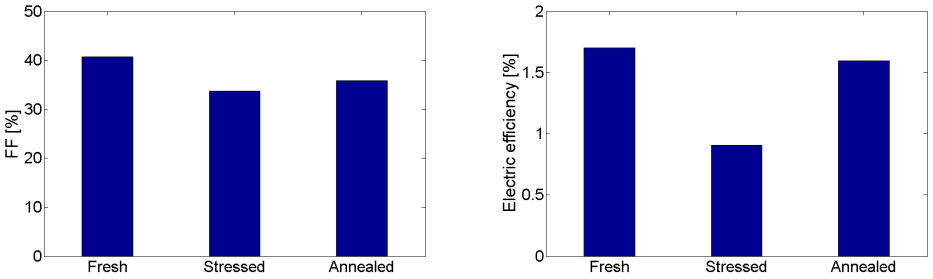

Figure 5.13: Effects of annealing on Fill Factor and Efficiency

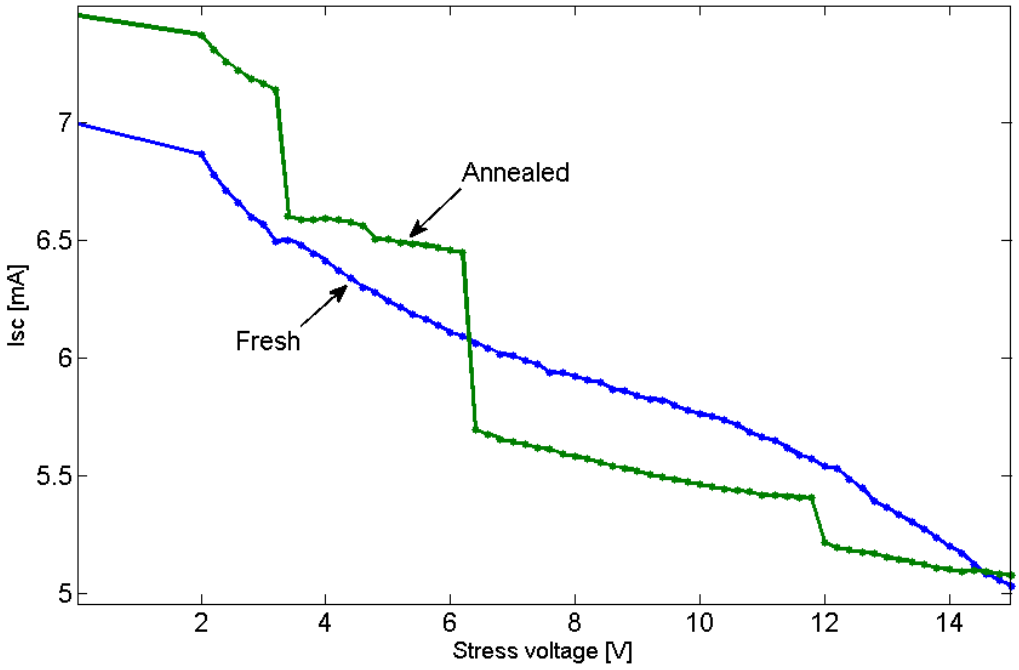

Figure 5.14: Isc kinetics of the same cell, before and after annealing. The stress was repeated using the same procedure. The annealed cell appears to be less stable than the fresh one.

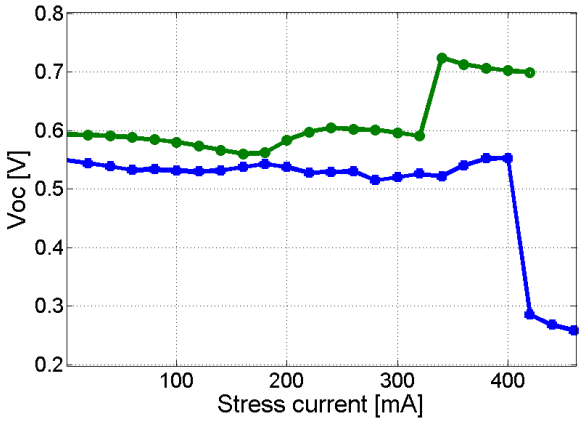

(a) Voc

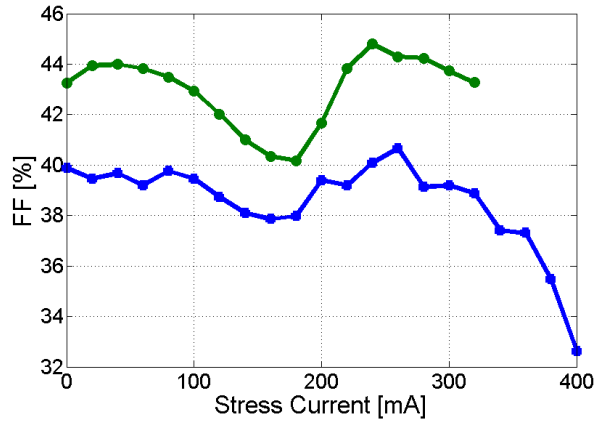

(b) Fill Factor

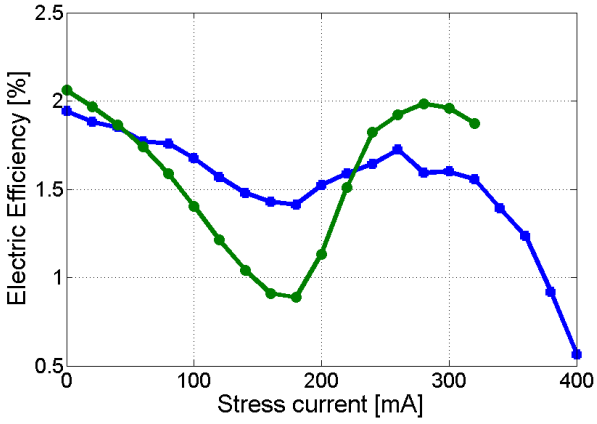

(c) Efficiency

Figure 5.15: Evolution of the figures of merit of the current-stressed cells.

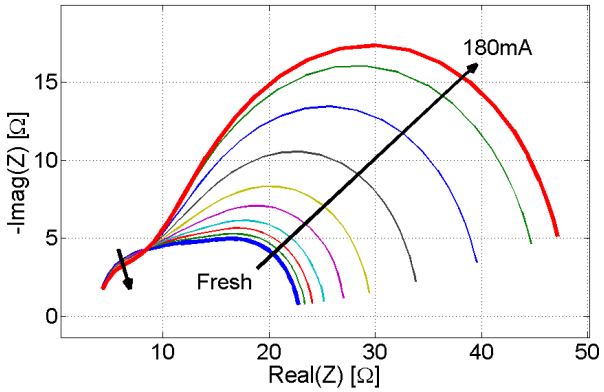

(a) First phase

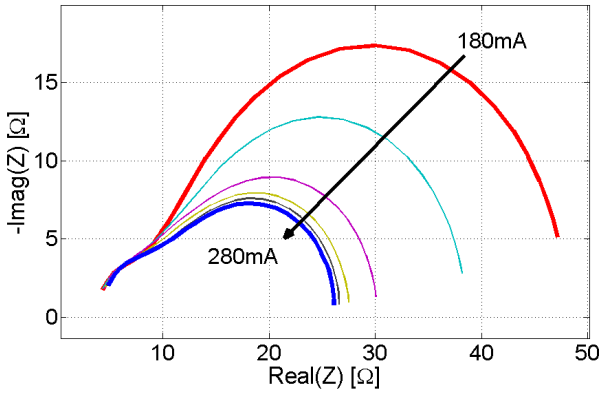

(b) Second phase

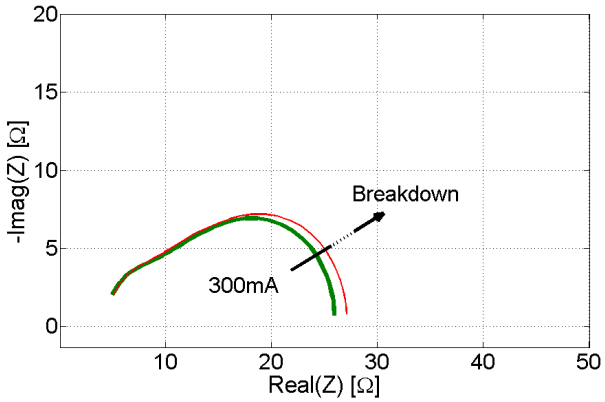

(c) Third phase

Figure 5.16: The impedance spectroscopy in the three phases of the stress.

5.2 Constant stress

To exclude the effects of the heating showed in the previous section, two more electric stresses were conducted on one cell each, the CVS (Constant Voltage Stress) and CCS (Constant Current Stress). Subsequently the stressed cells were put in a oven at 120°C for one hour and then stressed again with the same procedure.

In these stresses a constant voltage or current value is imposed to the cell, and the total stress time increases by 1.2 after each stress step, with a first step of 100 seconds. The voltage and current values were chosen in order to keep the dissipated power well under 200mW, so their temperature never became high enough to interfere with the degradation: the stress voltage during CVS was -9V, while the current during the CCS was 100mA.

The results of the CVS are quite different form those of the previous stresses: the performance of the cell didn't largely vary and, after the first 1000 seconds in which a steep decline arose, they settle and stayed unaltered until the end of the stress procedure. After the stress the cell was still functioning with only a little degradation in all its figure of merit, and it was then put one hour under 120°C to examine what effects would be induced.

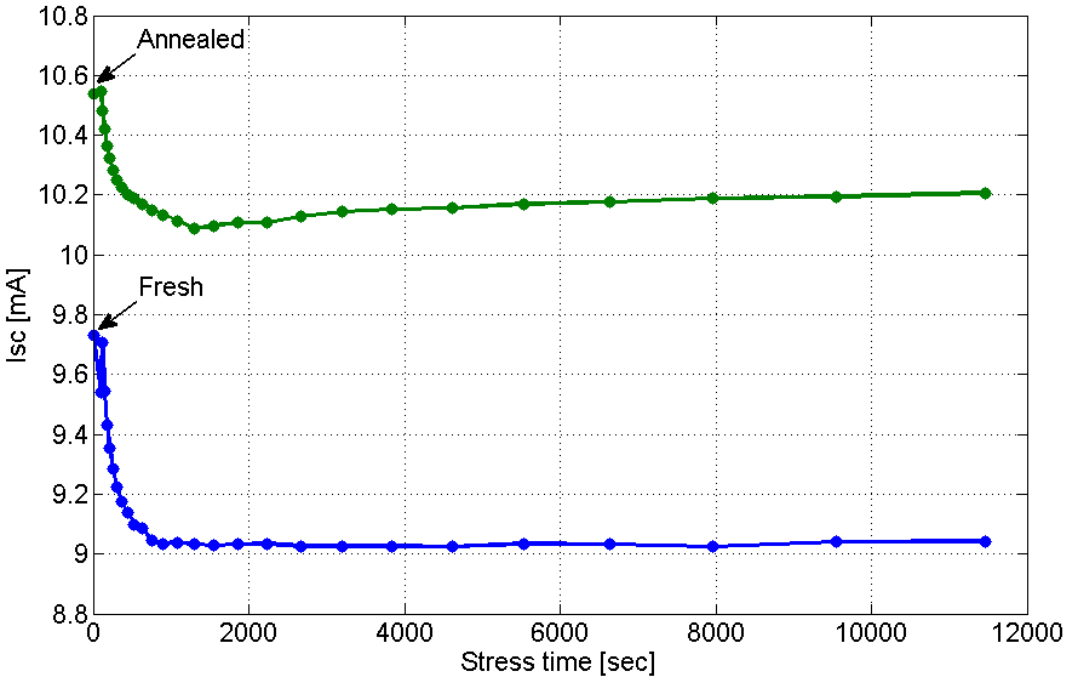

Figure 5.17: Isc kinetics of the cell stressed with 9V, before and after an heating sessione of 1 hour at 120°. The stress was repeated using the same procedure.

In figg. 5.17 and 5.18 on the facing page are shown the evolutions of the figures of merit: oddly, the Isc after the heating session exceeded the Isc of the fresh cell, and the response to the second stress was pretty much the same. Voc, Fill Factor and efficiency, though, behave differently: after the heating session they reached a value even lower than the one at the end of the first stress, and the following second stress actually improve them over time, to reach equilibrium again after 1000 seconds.

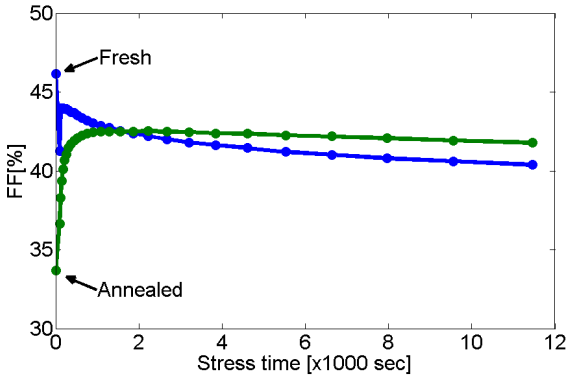

(a) Fill Factor

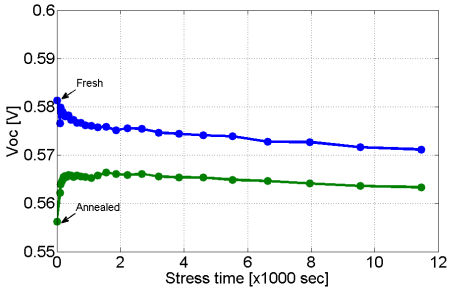

(b) Voc

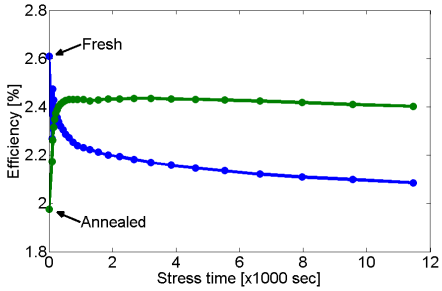

(c) Efficiency

Figure 5.18: Evolution of the figures of merit of the cell that underwent the CVS. During the second stress the performances actually improved compared with their starting value.

This strange behavior is explained by the I-V curves. During the first stress the degradation seems to be again due to a decrease of the generation rate or a growth of the recombination inside the active layer, because the curves didn't vary much their slope and Voc, but showed a more noticeable reduction in the short circuit current. In fig. 5.19 on the next page can be seen that after the 120°C hour the cell's I-V curve showed some kind of downward bending, which clearly decrease Voc and Fill Factor. In silicon cells this inflection is often interpreted in terms of a counterdiode, but *Glatthaar et al.* stated that, in organic solar cells, this can be attributed by a slow charge transfer at one of the electrical contacts of the absorber layer. Therefore the high temperature, differently from what happened from in the previous section, *damaged* the cell (and in particular the cell's contacts). The bending disappeared as the second stress proceeded, meaning that the temperature-induced damage wasn't permanent, but still in this case there weren't a real temperature-induced recovery.

The CCS didn't show the same behavior of the staircase current stress, since the 100mA current was chosen in order to keep the dissipated power under 200mW. Instead the results show a monotonic degradation that kept going until the end of stress, even if the total degradation didn't cause much damage. The hour under 120°C produced quite the same effects of the CVS: the performance greatly deteriorated and the following stress improved them, but they still didn't catch up with the performance of the fresh cell. If figg. 5.20 and 5.22 on page 67 are show the figure of merit.

The I-V curves followed the evolution of the CVS ones, and it's still present the

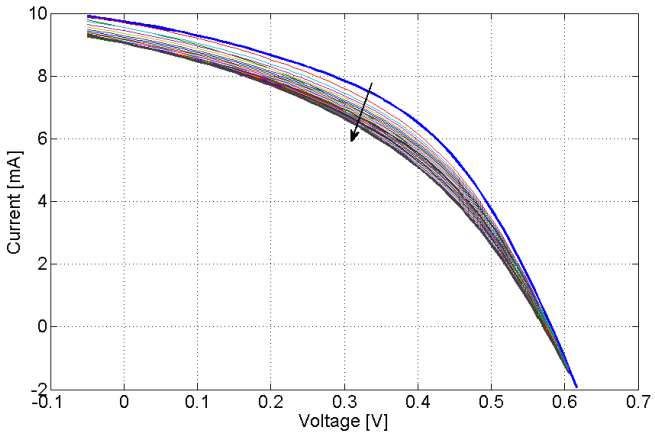

(a) First stress

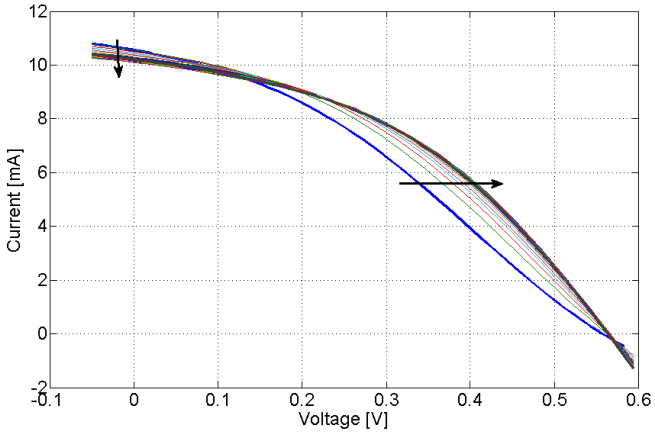

(b) Second stress

Figure 5.19: Evolution of the I-V curves during the first and second CVS stress. The second one was made after putting the cell under 120°C for 1 hour, and this caused the inflection which then disappeared during the stress.

bending caused by the high temperature. Again there wasn't any recovery due to the annealing, but considering the effect of the temperature on the contacts it could be due to the fact that 120°C is high enough to damage the cells besides inducing a recovery, and in these cases the former overcame the latter. In the following section the effect of two different temperatures on the solar cells are thus analyzed.

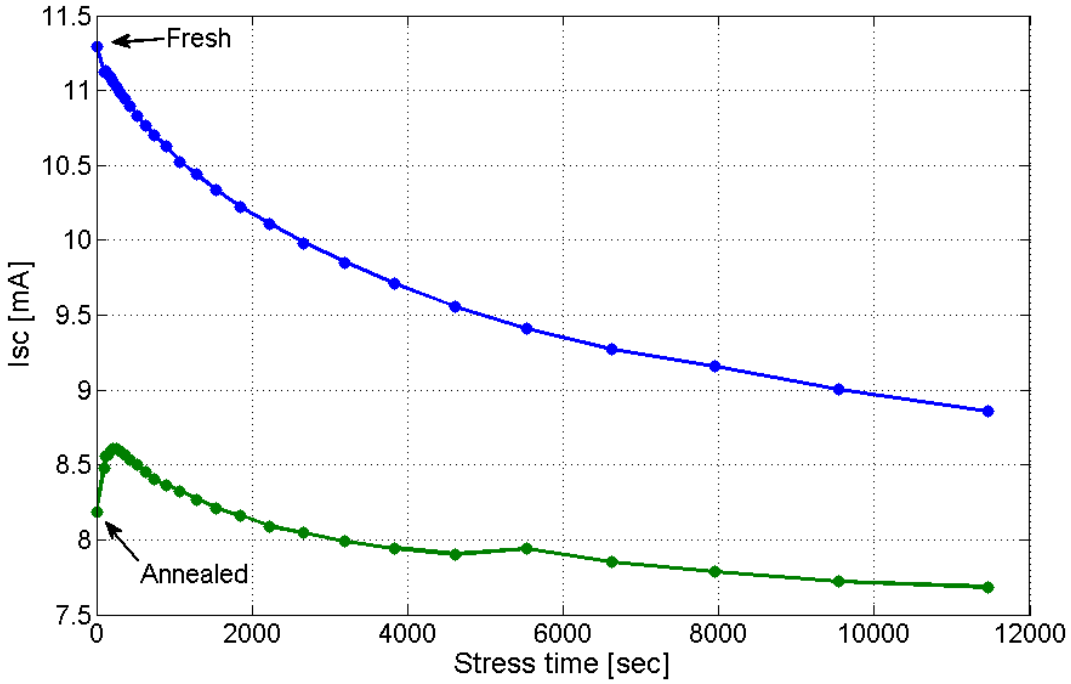

Figure 5.20: Isc kinetics of the cell stressed with 100mA, before and after an heating session of 1 hour at 120°. The stress was repeated using the same procedure. This time after the heating session there was a decrease of the Isc, which became even lower than what it was after the first stress.

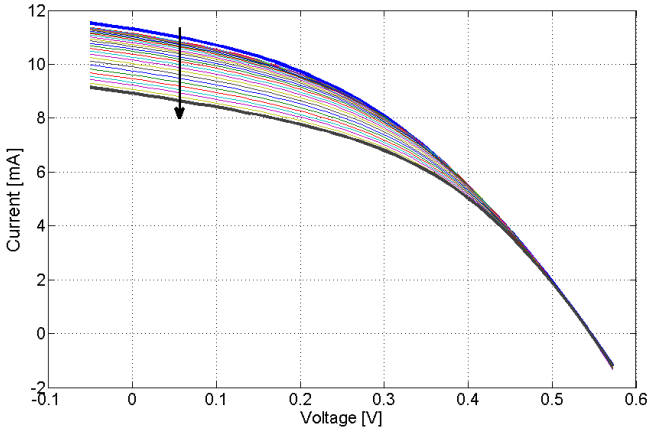

(a) First stress

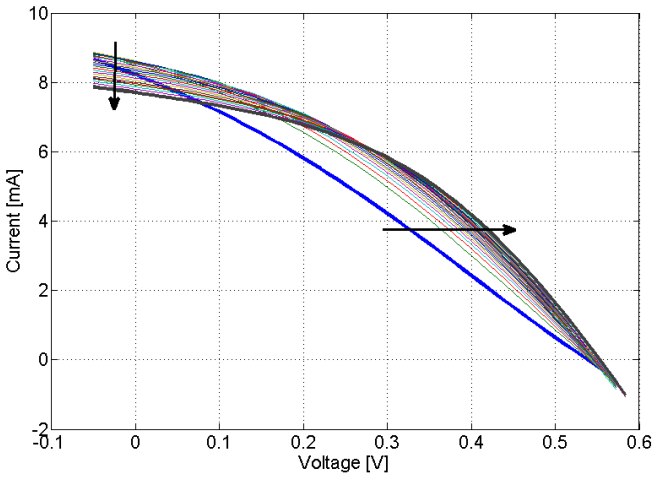

(b) Second stress

Figure 5.21: Evolution of the I-V curves during the first and second CCS stress. The second one was made after putting the cell under 120°C for 1 hour, and in this case too it caused the inflection of the curves.

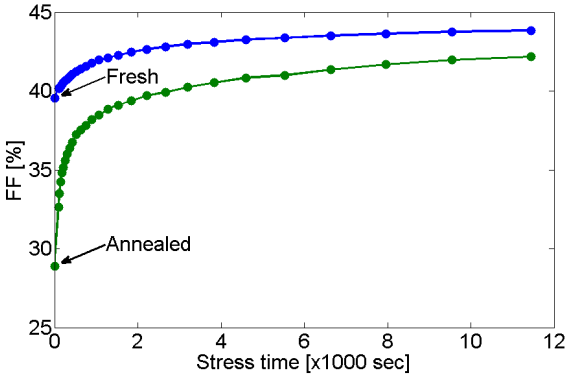

(a) Fill Factor

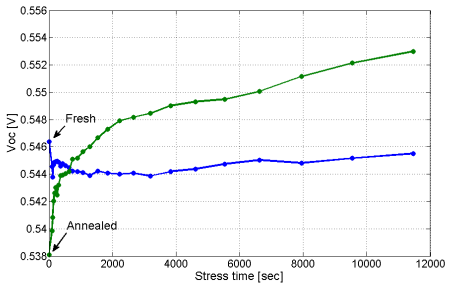

(b) Voc

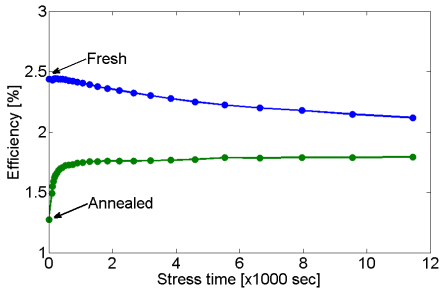

(c) Efficiency

Figure 5.22: Evolution of the figures of merit of the cell that underwent the CCS. During the second stress the performance improved in respect to their starting value, but overall they got worse compared to the fresh cell - with the exception of the Voc.

5.3 Thermal Stress

To execute the thermal stress the cells were put into an controlled oven, where the temperature is kept constant, in dark conditions and without any kind of bias. The duration of each step increased in order to double the total stress time after each step until 32 hours. The cells were characterized when they reached room-temperature. Two different stress were conducted, at temperature of 100°C and 120°C.

100°C

Since 100°C is not an extremely high temperature the decay seen in the CCS and CVS wasn't expected, and indeed the stressed cells don't seemed to alter very much. The most interesting thing is that after the first 1 hour-step the cell showed a significant improvement, proving the beneficial effects of a certain temperature, and only after that the degradation started. In fig. 5.23 is shown the evolution of the Isc of the two stressed cells, and the improvement after the first hour stands out.

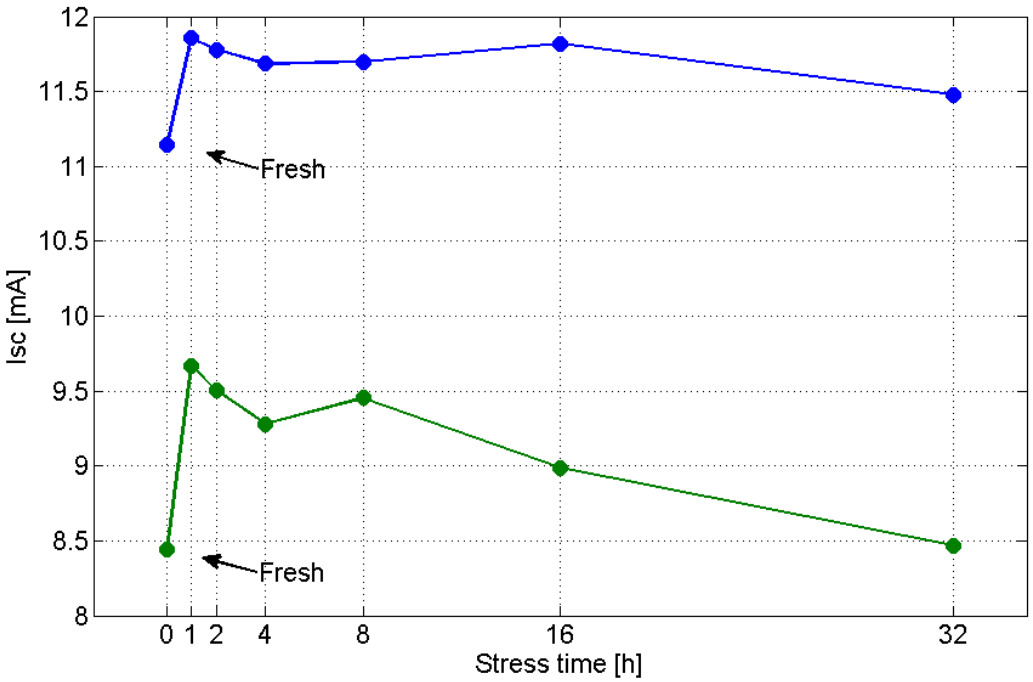

Figure 5.23: Isc kinetics of the two stressed cells (100°C). It's interesting to note the sharp improvement after the first hour, followed by a slow degradation.

After the first hour Isc and Voc don't change significantly; fill factor and efficiency, though, show some kind of fluctuation (5.25 on the facing page). The same fluctuation is visible in the I-V curves, but the general behavior is that as the stress goes on the curves tend to drop at lower voltages. (fig. 5.24).

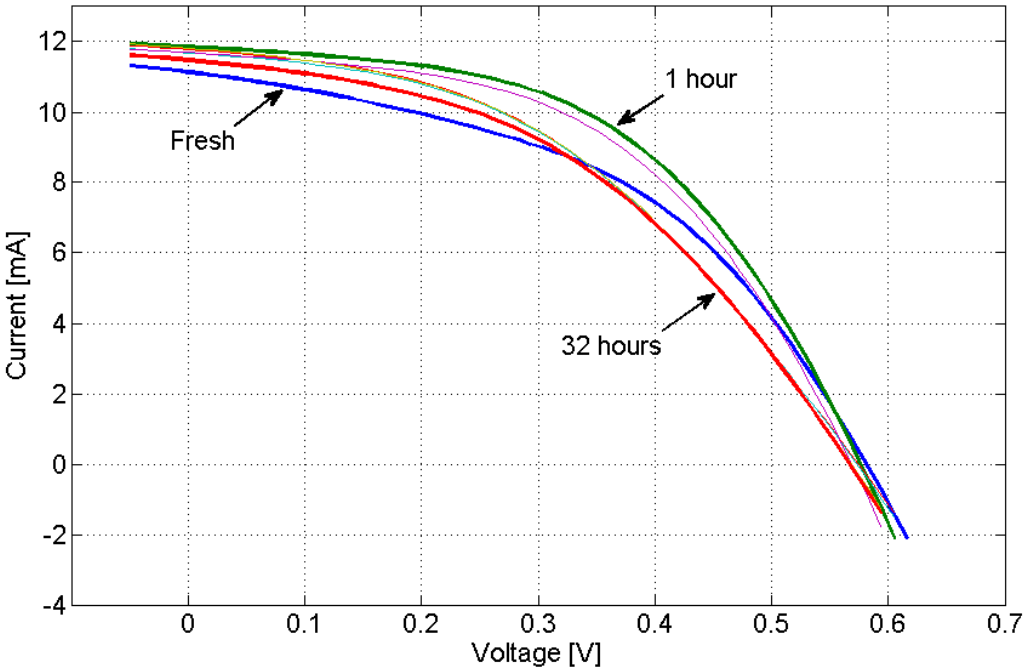

Figure 5.24: I-V curves after each step of the 100°C thermal stress.

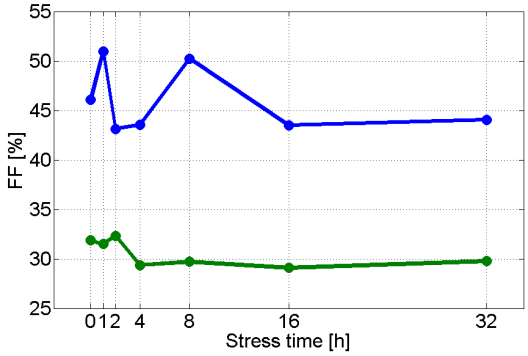

(a) Fill Factor

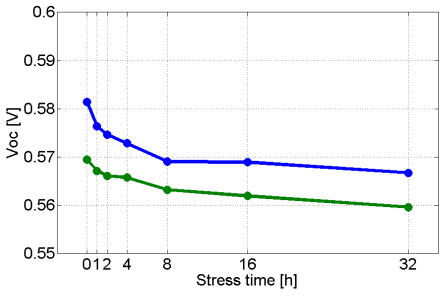

(b) Voc

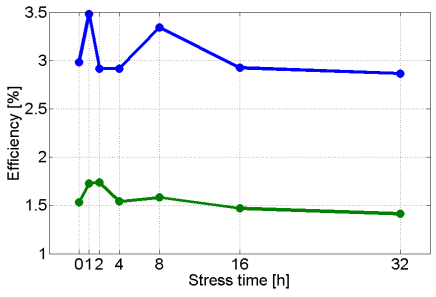

(c) Efficiency

Figure 5.25: Evolution of the figures of merit of the stressed cells (100°C)

120°C

Since the results of the previous electric stresses, it was uncertain if any improvement could affect the properties of the cells. In the end the cells underwent an immediate decay

even after the first step, except a cell – one that was already UV-degraded in DTU – which show little Isc recovering. It should be considered, though, that the previously heat-induced recovery was obtained from heavily-stressed samples or for self-heating session. A stress time of one hour under 120°C could be suitable for some magnitude of damage but too intense for a almost fresh cell. The temperature and the time required to an annealing session could thus depend on the entity of the damage. Moreover in the self-heating process the heat begins *inside* the blend and doesn't spread homogeneously all over the cell, but remains mostly in the active layer. During the stress the temperature is constant and homogeneous over the entire cell, therefore different results are justified.

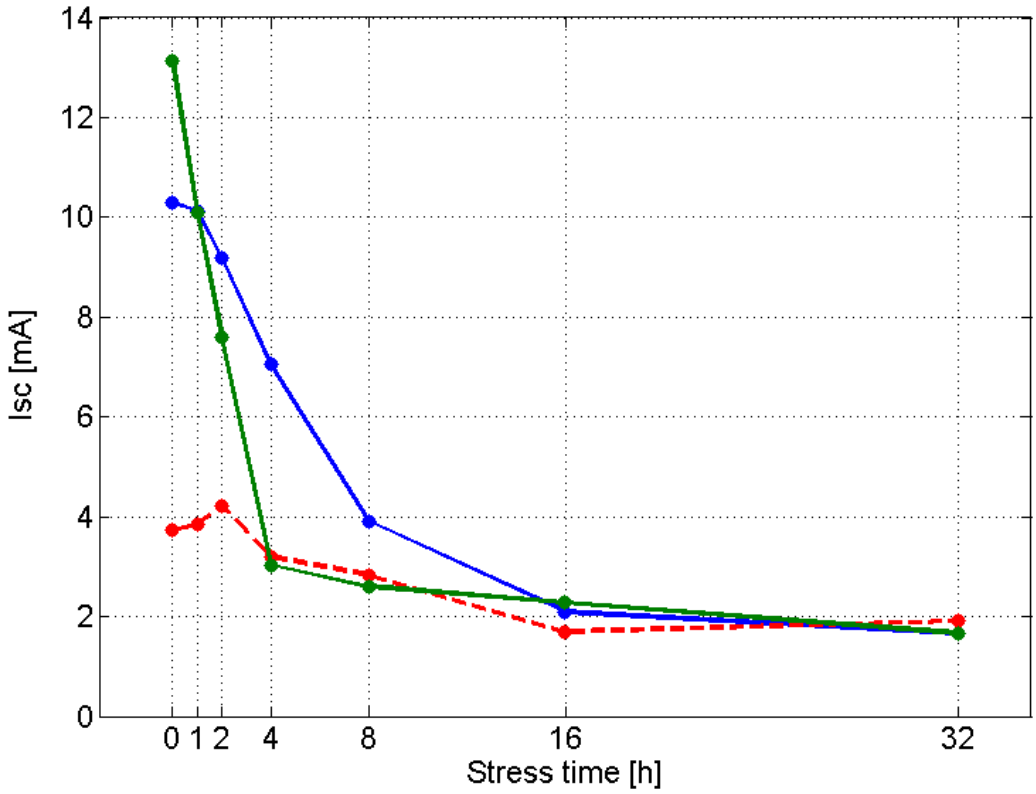

Figure 5.26: Isc kinetics of the three stressed cells (120°C). After the first step the cells are already degraded, with the exception of the one already UV-degraded in DTU (dashed line). This could mean that either the temperature or the stress duration are too high for fresh cells, while it has been seen that they recover the one electrically stressed.

Looking at the evolution of the figures of merit (fig. 5.26 and 5.27 on the facing page) it can be seen that after 8 hours of stress the characteristics of the cells reach a "stable point". The Isc, for instance, lowered considerably and settled down at around 2mA. It's worth noting that the "stable points" of the two fresh cells are the same in every figure of merit, independently from their starting value.

The I-V curves show again the particular behavior already seen in CVS. The more the stress goes on, the more a *kink* appear near Voc, that is the inflection of the I-V curve that reduces the fill factor. Glatthaar found that it coincides with a large capacitance for low frequencies, as additional charges injected from the good contact are accumulated at the

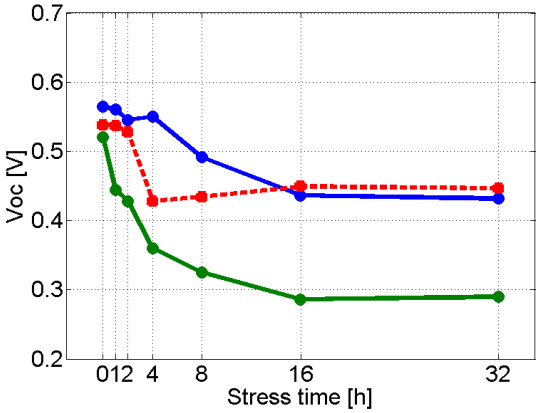

(a) Voc

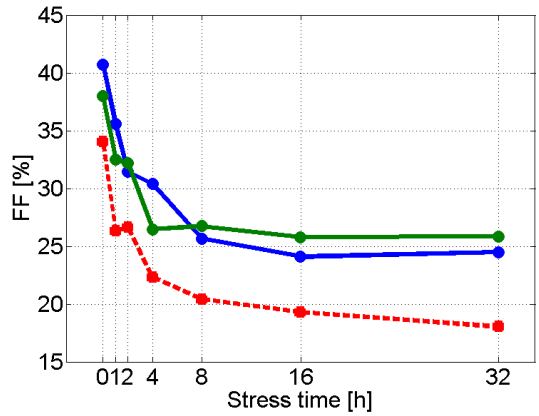

(b) Fill Factor

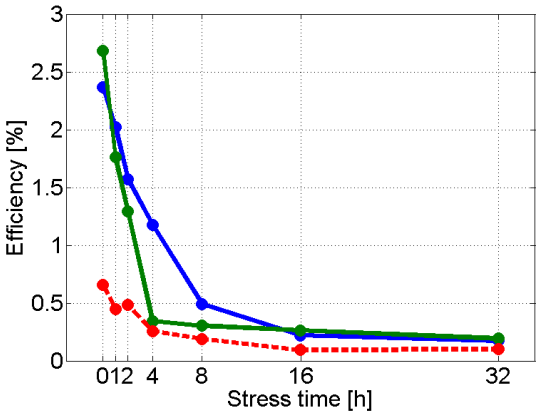

(c) Efficiency

Figure 5.27: Evolution of the figures of merit of the stressed cells (120°C)

blocking contact. This should coincide with the debye capacity used in one of the possible model showed before. Looking at the impedance spectroscopy made on the cell that is more affected by these inflections, it can be seen that the peak of the low frequency lobe actually shifts towards lower frequencies, meaning that its capacity is indeed increasing. This could mean that the temperature of 120° is high enough to cause, in addition to the

annealing of stressed cells, a degradation of the cell's contacts.

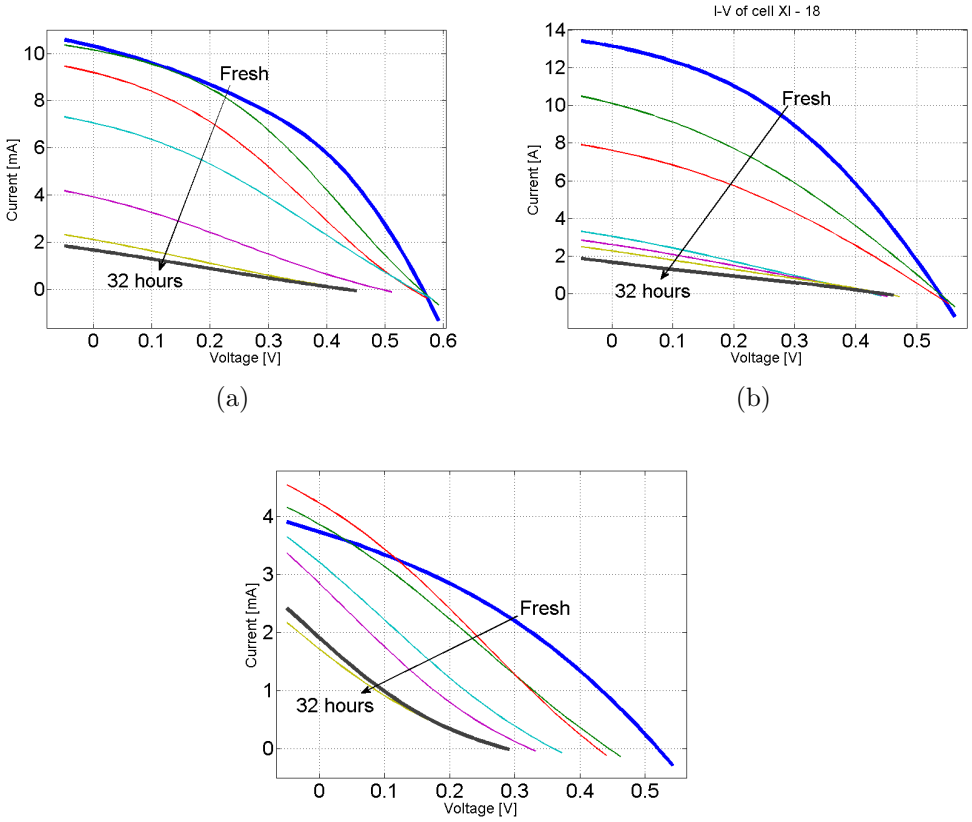

Figure 5.28: Evolution of the I-V curves during the stress. In a) and b) are the curves of the two cells which were fresh, while in c) are the curves of the cell UV-degraded in DTU.

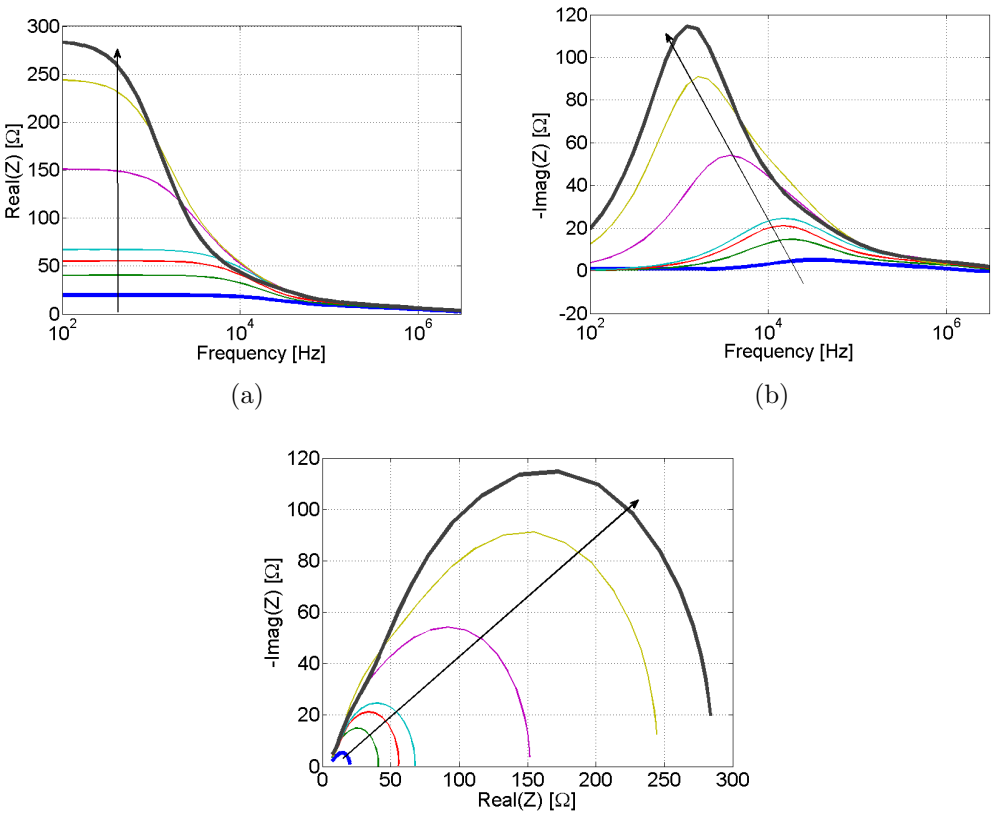

Figure 5.29: Impedance spectroscopy of the cell which is more affected by the inflections in the I-V curves.

Chapter 6

Conclusions

The effects of electric stresses were analyzed. The induced degradation is to be attributed to a decrease of the generation rate, either due to the formation of exciton quenching centres or to a growth of the recombination *inside* the active layer, and to the formation of *shunts* between anode and cathode. During the current staircase stress the cell showed a peculiar behavior, and a certain recovery appeared in the middle of the process. This recovery is due to the self-heating of the cell caused by the power dissipation, which induces the annealing. CVS and CCS were conducted under conditions that prevented the self-annealing effect, and the stresses were repeated after an hour under 120°C, to trying and reproduce the recovery. This tests showed that a temperature of 120°C induces also a degradation of the cell, which may exceed the recovery. Test were made under 120° and 100°, to reproduce the effect of the annealing. After 1 hour under 120° the degraded cells showed both recovery and damage, the latter being attributed to the damage of the electric contacts. A temperature of 100° proved to be more appropriate, as a session of one hour could improve the performances of different cells without drawbacks. These results could open new scenarios in the evaluation of the lifetime of polymeric solar cells. Inorganic silicon solar cells can undergo an annealing process only at temperatures of a few hundred Celsius degrees, and therefore their operating temperature under sun (that can be higher than 80°C) is only a factor of degradation. As we have seen, however, the annealing temperature of polymeric solar cells is not so far from their operating temperature under sun, and that should be considered while evaluating their life time.

Bibliography

[1] Martin A. Green, *Silicon Photovoltaic Modules: A Brief History of the First 50 Years.*

[2] Adolf Goetzberger, Christopher Hebling, Hans-Werner Schock, *Photovoltaic materials, history, status and outlook.*

[3] European Photovoltaic Industry Association, *Global market outlook for photovoltaics 2014-2018.*

[4] C. Julian Chen, *Physics of Solar Energy.*

[5] Andrea Cester, *Elettronica organica e molecolare.*

[6] R. Farchioni, G. Grosso, *Organic Electronic Materials: Conjugated Polymers and Low Molecular Weight Electronic Solids.*

[7] Material matters vol. 4 no. 3. *Organic and Molecular Electronics*

[8] Sourabh Dongaonkar, Muhammad A. Alam, *End to End Modeling for Variability and Reliability Analysis of Thin Film Photovoltaics.*

[9] Hybridization - how does carbon form tetrahedral structures?
http://www.ntu.ac.uk/cels/molecular_geometry/hybridization/Carbon/index.html.

[10] Gamry Instruments, *Basics of Electrochemical Impedance Spectroscopy.*